Flexing piezoelectric diphenylalanine–plasmonic metal nanocomposites to increase SERS signal strength

Sawsan Almohammed [a, b], Agata Fularz [a], Fengyuan Zhang [a, b], Diana Alvarez-Ruiz [a], Frank Bello [c], David D. O'Regan [c], Brian J. Rodriguez * [a, b], and James H. Rice * [a]

[a]*School of Physics, University College Dublin, Belfield, Dublin 4, Ireland*
[b]*Conway Institute of Biomolecular and Biomedical Research, University College Dublin, Belfield, Dublin 4, Ireland*
[c]*School of Physics, AMBER and CRANN Institute, Trinity College Dublin, The University of Dublin, Dublin 2, Ireland*

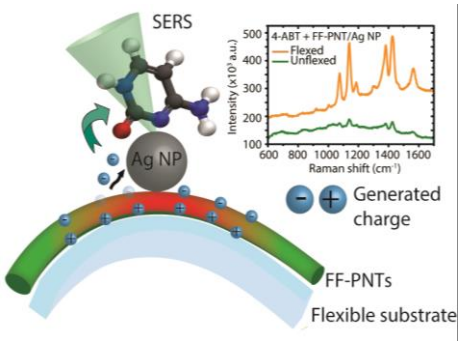

Abstract
Piezoelectric quasi-1D peptide nanotubes and plasmonic metal nanoparticles are combined to create a flexible and self-energized surface-enhanced Raman spectroscopy (SERS) substrate that strengthens SERS signal intensities by over an order of magnitude compared to an unflexed substrate. The platform is used to sense bovine serum albumin, lysozyme, glucose, and adenine. Finite-element electromagnetic modelling indicates that the signal enhancement results from piezoelectric-induced charge, which is mechanically-activated via substrate bending. The results presented here open the possibility of using peptide nanotubes on conformal substrates for in situ SERS detection.

Keywords
Peptide, Diphenylalanine, Nanostructures, Surface-enhanced Raman spectroscopy, Piezoelectric, Self-energized.

Introduction
Flexible surface-enhanced Raman spectroscopy (SERS) substrates, such as those based on polymers, are lightweight and deformable, enabling them to be wrapped onto curved surfaces or cut into arbitrary shapes and sizes.[1–4] Such design features enable the substrate to intimately contact arbitrary surfaces for in situ and onsite detection. Flexible substrates can be integrated into wearable devices with wireless communications for personalized health monitoring, and be customized for point-of-care diagnostics.[1–4]

The combination of SERS-active structures with piezoelectric polymers has been reported to boost SERS signals when the substrate is compressed to generate a negative electric potential on the substrate surface.[5] The surface potential then injects electrical energy into the plasmon-active metal nanostructures, resulting in heightened SERS intensities as the band structures equilibrate following the change in charge state. Such approaches to boosting SERS signal intensities have been applied to piezoelectric polyvinylidene fluoride (PVDF) and silver nanowire composite films. These self-energizing SERS substrates have been activated by pressing the substrate with a finger to enable a 3-fold increase in SERS signal intensity.[5]

Bio-inspired materials such as diphenylalanine peptide nanotubes (FF-PNTs) are attractive alternatives to polymers as they can present a more environmentally-sustainable piezoelectrical material source.[6] Self-assembled FF-PNTs have emerged as attractive materials that possess unique advantages such as low cost,[6] mechanical rigidity,[7,8] and also thermal and chemical stability.[9–12] In addition, FF-PNTs are piezoelectric[13–16] possessing piezoelectric properties comparable to conventional piezoelectric materials such as zirconate titanate, lithium niobate, and barium titanate.[17,18] Owing to the piezoelectric nature of FF-PNTs, they have been used in energy harvesting applications.[19–21] The fabricated FF-PNT-based piezoelectric energy harvesters can generate a voltage, current, and power of up to 2.8 V, 37.4 nA, and 8.2 nW, respectively.[19] Here, we show that through mechanical flexing of a thin film of aligned piezoelectric FF-PNTs and plasmon-active silver nanoparticles (Ag NPs), we boost SERS intensity by approximately an order of magnitude for a range of probe molecules. This work highlights the use of FF-PNTs in conjugation with Ag NPs for the fabrication of well-defined functional nanocomposites for ultrasensitive (down to femtomolar) SERS sensing. Additionally, the composite properties are potentially applicable for the design of novel flexible energy harvesting and flexible electronic devices.

Results

PNTs and Ag NPs were aligned using ultraviolet (UV) ozone treatment of a polyvinyl substrate through a physical mask separated by 0.5 cm, following a procedure reported elsewhere.[22] UV/ozone treatment of plastic materials leads to the generation of an oxide layer on the surface, making it more hydrophilic.[23,24] The wettability difference between the polyvinyl surface (contact angle (CA) of 68.3 ± 1.8°) and the resulting oxide layer (CA = 4.3 ± 1.2°) promotes FF-PNT alignment during self-assembly.[22,25–29] Scanning electron microscopy (SEM) was used to characterize the aligned FF-PNT/Ag NP template (Figs. 1(a) and S1-S2). The diameter of the FF-PNTs was determined to be 3.5 ± 1.2 μm from n = 30 FF-PNTs. Ag NPs can be observed to aggregate in localized regions on and around the FF-PNTs due to strong chemical and electrostatic interactions.[22,25–29] Additionally, the template remains intact following the addition of the probe molecule solution (Fig. S1). Fig. 1(b) shows the bending rig and a schematic illustration of the bending of the aligned FF-PNT/Ag NP flexible substrate. A comparison of energy-dispersive X-ray spectroscopy images before and after bending revealed that the aligned FF-PNTs did not undergo chemical change (Figs. S2). Atomic force microscopy (AFM) and piezoelectric force microscopy (PFM) confirmed the structure and piezoelectric response (deformation in response to an applied electric field) of the FF-PNTs (Fig. 1(c)). The piezoelectric response (bright contrast from FF-PNTs in the PFM amplitude image) was found to depend on the orientation of the FF-PNTs with respect to the cantilever, as reported before.[19,21] When

the cantilever was oriented orthogonal to the FF-PNT, a strong shear component of the piezoelectric tensor, d_{15}, attributed to the in-plane signal was determined to be 27.5 ± 0.4 pm/V (Fig. S3) from local measurements, similar to previously reported values.[19] Regions exhibiting FF-PNTs having the same polarization direction were identified from the PFM phase image in Fig. 1(c). Flexing the nanocomposites is expected to generate both compressive and tensile strains,[19,20] as shown in the supplementary information, Table S1.

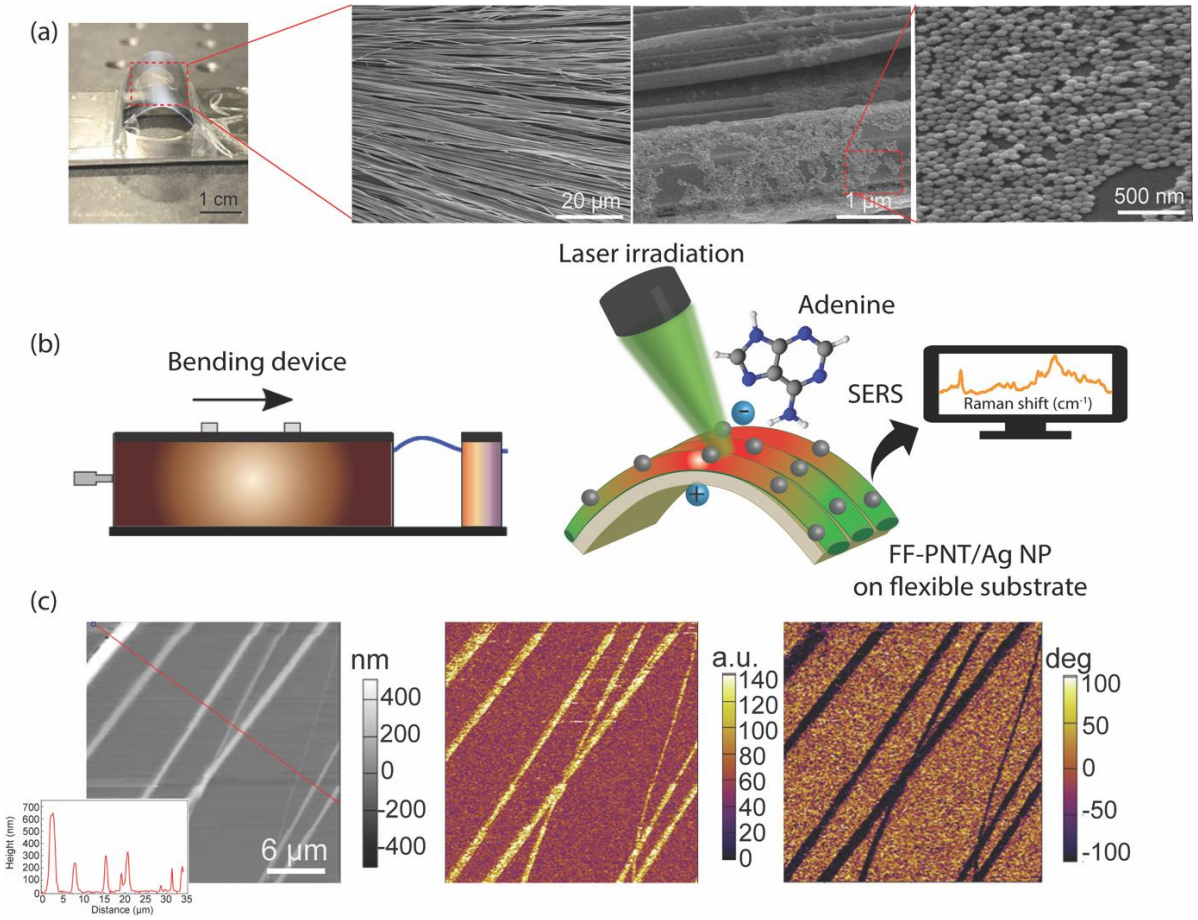

Fig. 1. (a) Photograph and SEM images of an aligned, flexed FF-PNT/Ag NP substrate. (b) Schematics of the device used to flex the substrate and a SERS experiment with a flexed FF-PNT/Ag NP substrate. (c) AFM topography (left), lateral PFM amplitude (middle), and lateral PFM phase (right) images. The insert in the topography image is the height profile corresponding to the red line in the topography image. The average height of the FF-PNTs in this image is 281 ± 101 nm. The bright color in the lateral PFM amplitude image correspond to the FF-PNTs visible in the topography image, while the dark color in the lateral PFM phase image indicates these nanotubes have the same polarization direction.

We examined the influence of flexing the substrate on the SERS intensity. Flexing the nanocomposites generates both compressive and tensile strains, of equal magnitude on the top and bottom surfaces of the sample, respectively. Assuming uniaxial strain, the bending stress was calculated from $\sigma_x = E\varepsilon_x$, where E is the Young's modulus of the composite and ε_x represents contributions from compressive and tensile strains (as outlined in the supplementary information, Table S1). The influence of flexing the

substrate on the SERS intensity using the probe molecule 4-ABT was first investigated (Fig. 2). 4-ABT is not in resonance with the 532 nm laser excitation wavelength used, having an absorption band in the UV region of the spectra, as shown in (Fig. S4).[30–32] Flexing the FF-PNTs convex (to apply tensile strain) with respect to the laser (shown schematically Fig. 2(d)) to generate 0.12 GPa of stress resulted in the SERS spectral intensity increasing by an order of magnitude (peak-to-peak ratio) for four different Raman bands (Figs. 2(e,f) and S5). Increasing the generated stress above ~0.12 GPa resulted in a reduction in the peak-to-peak ratio signal intensity for all bands (Figs. 2(f) and S5). In contrast, flexing the FF-PNTs concave to apply compressive strain (shown schematically Fig. 2(a)) shows comparatively no increase in SERS signal intensity (Fig. 2(b,c)).

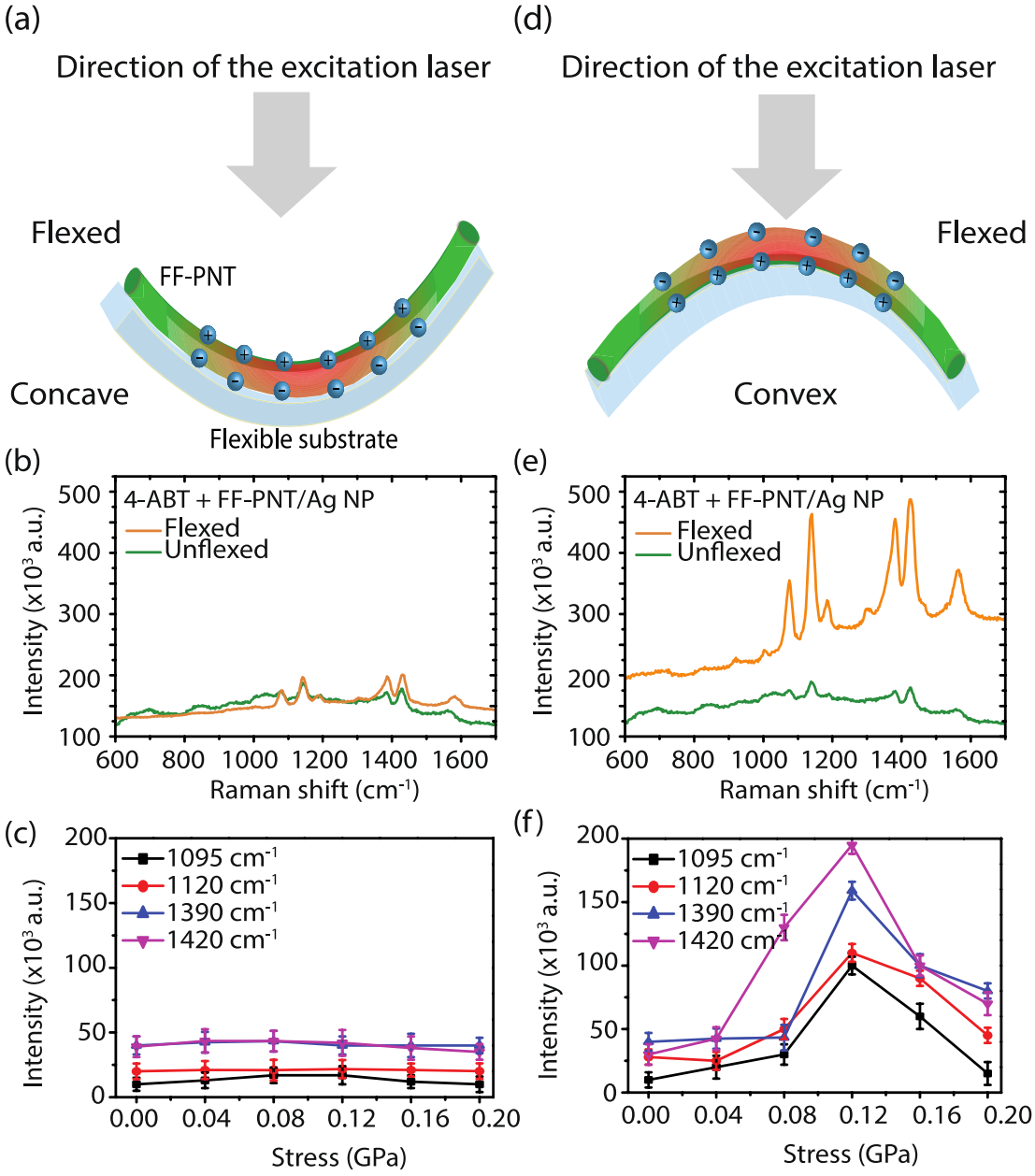

Fig. 2. SERS measurements of the probe molecule 4-ABT (10^{-6} M) using the aligned FF-PNT/Ag NP flexible substrate. Schematic drawings of the substrate flexed to orientations (a) concave (compression strain) and (d) convex (tensile strain) with

respect to the direction of the excitation laser. Shown in red are the areas where the generated stress is maximized, generating surface charge through a piezoelectric strain and/or a flexoelectric strain gradient. (b,d) SERS data recorded from a sample flexed in the orientation shown in (a). (e,f) SERS data recorded from a sample flexed in the orientation shown in (d). SERS spectra shown in (b,e) were recorded before and during flexing, with the FF-PNTs flexed to generate a calculated stress of 0.12 GPa. The Raman signals are averaged for six measurement locations. (c,f) Plots of SERS signal intensity versus the degree of strain.

Next, we investigated meso-tetra (N-methyl-4-pyridyl) porphine tetrachloride (TMPyP), possessing a Q-band ($a_{2u} \rightarrow e_{gx}$) electronic transition in resonance with the excitation laser (λ_{ex} = 532 nm) (Fig. S4). Despite being in resonance, TMPyP showed similar behavior to that observed for 4-ABT (Fig. S6). When using 4-ABT, strong coupling between 4-ABT and the template can result in chemical enhancement, as previously reported.[26] SERS spectra for TMPyP on the FF-PNT/Ag NP substrate before bending show Raman bands arising from TMPyP, such as bands at 1249 cm^{-1} (C-pyrrole bending), 1451 cm^{-1} (C–C stretching), 1573 cm^{-1} (C–C stretching), and 1639 cm^{-1} (pyrrole bending).[25,33] The peak-to-peak Raman band intensity increased 5-fold for all bands when flexing the FF-PNTs convex with respect to the laser excitation to generate 0.12 GPa of stress. Increasing the generated stress over ~ 0.12 GPa resulted in a reduction in the peak-to-peak ratio signal intensity (Fig. 2(c)). TMPyP concentrations as low as 10^{-11} M and 10^{-9} M have been detected after using FF-PNT/Ag NP and FF-PNT/Au NP templates, respectively, after bending (0.12 GPa) (Fig. S7). At low concentrations, FF-PNT breathing mode bands started to appear at 1000 cm^{-1} and 1003 cm^{-1}.

During substrate flexing, it is expected that the strain applied to the FF-PNTs activates a piezoelectric potential by converting the FF-PNT deformation into stored electrical energy, which produces a negative electric potential on the surface of the FF-PNTs.[5,19,20] The surface potential then injects electrical energy into the plasmon-active metal nanostructures. Finite-element electromagnetics simulations were undertaken to probe the effect of the piezoelectricity-driven electrical charge migration from the FF-PNT to the metal nanostructures on SERS signal intensities (Fig. 3).

The initial SERS intensity level arising from the metal nanoparticles through the electromagnetic field enhancement was first calculated. We then simulated the piezoelectric-driven boost to SERS signal intensities by assessing how changing the FF-PNT surface uniformly affects the SERS signal levels. A plot of the SERS enhancement factor, G (as defined in the experimental section), resulting from a variable uniform surface charge applied on the FF-PNT was generated (Fig. 3(a). This plot shows the effect of surface charge on the SERS intensity relative to the Ag NP SERS enhancement with zero applied surface charge. This shows that the SERS signal level is enhanced with increasing net surface charge. In contrast, the SERS intensity is lowered for slightly negatively charged FF-PNTs. Under this condition, the applied charge acts to cancel the charge build-up that is present ordinarily at the FF-PNT–Ag NP interface due to binding interactions. Overall, the plot (Fig. 3(a)) shows that with the increasing charge there is, in general, an increase in SERS signal intensity, which is an unsurprising result in the model used. More interestingly, next, we modeled how SERS enhancement is affected when increasing the surface charge in Ag NP-decorated FF-PNTs. This gave an indication of how the piezoelectric

potential supplied through flexing the FF-PNT affects the SERS signal level. Fig. 3(b) depicts the same boost to the SERS enhancement G, as with Fig. 3(a), now averaged over applied charges (positive and negative, assuming overall charge neutrality of the NP-decorated FF-PNT surface). Under such conditions, which are reasonable for a linear piezoelectric where the induced charge resides on the surface of the FF-PNT, we predict that SERS can be boosted in principle by a factor of >20.

Simulations were then made to assess the impact of the charge arising from the FF-PNT interacting with the dielectric response of the Ag NPs (Fig. 3(c)) to create an electromagnetic enhancement of the Raman signal. The possibility of enforced charge transfer to Ag NPs is not explicitly included in our calculations. Instead an applied charge was fixed to the FF-PNT surface and the intrinsic charges of the system were free to arrange. Here, we investigated the electric field 'hot-spot' effect of the Ag NPs on the SERS signal in terms of an efficiency multiplier, i.e., the predicted multiplicative boost in SERS due to the presence of Ag NPs as a function of the FF-PNT surface charge. Following the transfer of negative charge from the FF-PNT to the Ag NP (or indeed to the underside of the FF-PNT or to its ends), holes will be present on the surface of the FF-PNT, as simulated in the shaded region in Fig. 3(c) and shown schematically in Fig. 3(d). During this process, the SERS intensity increases. It may also increase due to a separate chemical effect (see below), which is not simulated here. The SERS intensity then drops at a point when the hole concentration is large enough to 'pull-back' the electron charge on the Ag NP, causing the electrons to transfer from the Ag NP to the FF-PNT until equilibrium is reached. Inspection of the experimental data (Fig. 2(f)) shows that increasing the generated stress up to 0.12 GPa results in a SERS intensity increase, while flexing the substrate beyond this value results in a reduction in SERS signal intensity. The further maximum SERS enhancement (due to Ag NP) occurs when around 20 electron charges are added to an Ag NP, in our idealized model. The charging of the FF-PNT is qualitatively representative of the SERS electromagnetic enhancement process. This is distinct but not easily disentangled from the additional chemical enhancement mechanism.[25–29] Electron accumulation on the surface of the FF-PNT yields a predicted (Fig. 3(c)) electromagnetic reduction in SERS signal intensity (relative to simulations where the Ag NP is absent). Flexing the substrate in the orientation shown in Fig. 2(d), i.e., in the opposite direction, results in a small increase in SERS intensity as the transfer of holes does not influence the SERS signal intensity to the same extent. A recent study of aligned FF-PNTs reported that convex bending of aligned FF-PNTs created a negative output voltage and current, while concave bending resulted in a positive output voltage and current,[19] demonstrating the significance of bending orientation on the SERS intensity via the piezoelectric charge.

In brief, the electromagnetics results show that the piezoelectric-based electric field induces internal fields in the Ag NP that work cooperatively (right-hand colored panel of the plot in Fig. 3) to boost the SERS signal. Generally, the effect of adding a positive charge to the FF-PNT surface results in an enhancement in the SERS signal. In contrast, when a negative charging of the FF-PNT surface is undertaken, a reduction in SERS signal is produced. When 20 positive charges are present at the FF-PNT surface, the maximum SERS signal is produced. Adding further positive charges reduces the SERS signal intensity, which causes a reduction in the cooperative piezoelectric-based field and the internal field of the Ag NPs.

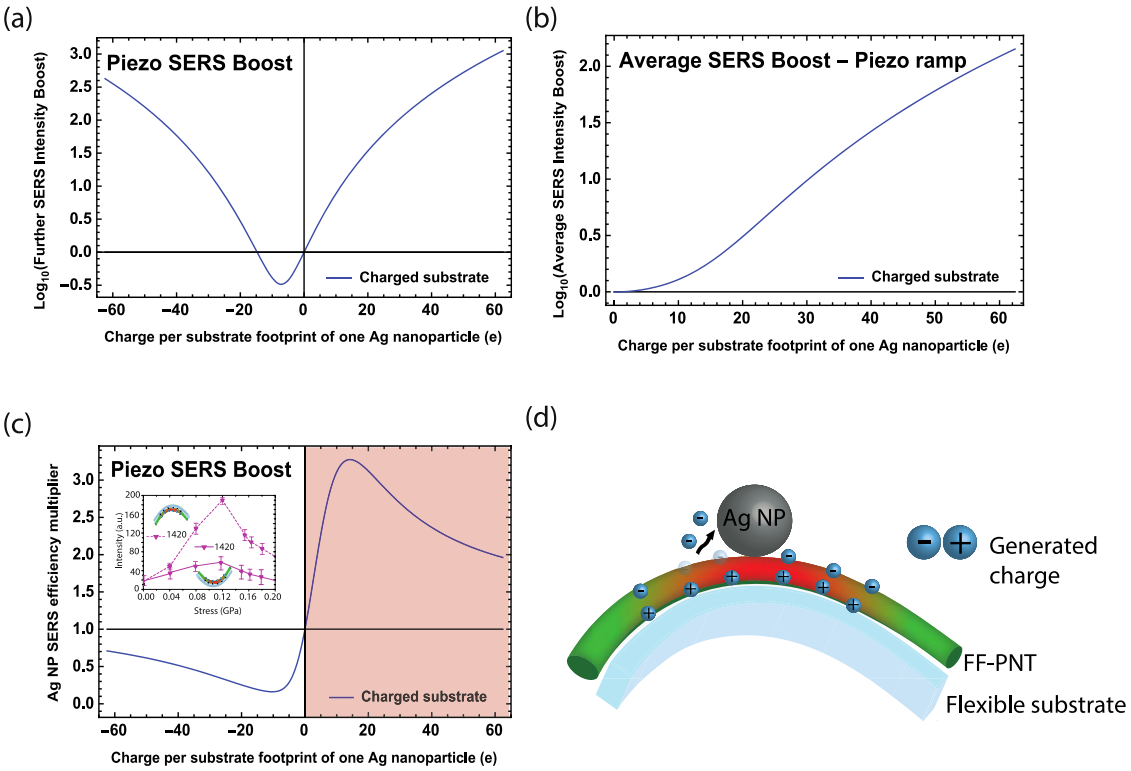

Fig. 3. Simulations of SERS enhancement on FF-PNT/Ag NP substrates with charging. (a) Modelled piezoelectric-driven boost to the SERS enhancement, G, in the presence of a square-lattice monolayer of Ag NPs. A plot of the multiplicative boost to the SERS enhancement factor, G, resulting from a variable applied uniform surface charge on the FF-PNT. The Ag NP SERS enhancement with zero applied surface charge is set to unity. (b) Averaged piezoelectric-driven enhancement boost. In order to model how SERS enhancement might be affected, on average, by a piezoelectric FF-PNT, we simulated a linear ramp to its surface charge density. The x-axis represents the maximum charge density magnitude and the y-axis is the average boost to the SERS enhancement, G, along the nanotube, divided by the G calculated for Ag NPs with zero applied FF-PNT surface charge. (c) Simulation of the multiplicative change in the Ag-induced SERS enhancement when a uniform FF-PNT surface charge is added. Shown on the left side of the plot is simulated data when the FF-PNT surface is negatively charged. Shown on the right-hand side (shaded) is simulated data when the FF-PNT surface is positively charged. Note in each case that the generated values apply to a highly idealized geometry and an optimal incident wavelength; we place emphasis only on the qualitative predictions of the model. When there is no bending, the SERS efficiency is set to a relative value of 1. Shown for reference (inset) is experimental data taken from Fig. 2. (d) Illustration of a charged FF-PNT in the presence of an Ag NP with holes and electrons. When electrons move from the FF-PNT to the Ag NP, hole states remain on the FF-PNT.

As a further check on the proposed piezoelectric mechanism, studies comparing piezoelectric nanotubes (FF-PNTs), non-piezoelectric nanotubes (Cyclo-FF), and low-piezoelectric nanotubes (Cyclo-WW) were also undertaken using 4-ABT (Figs. S8–S10). We first characterized the structures using SEM, UV-Vis, and FTIR, as shown in (Figs. S8 and S9). Raman spectra (Fig. S10) show that Cyclo-WW structures do not enhance the SERS signal to the same extent as when the piezoelectric FF-PNTs are

used. In addition, there is no enhancement when using non-piezoelectric Cyclo-FF. The influence of bending on FF-PNTs with and without Ag NPs in the absence of the probe molecule was also investigated (Fig. S11). The degree of flexing was chosen to match the optimum degree of flexing found in Fig. 2, e.g., 0.12 GPa. The Raman spectrum for the substrate in absence of both probe molecule and Ag NPs (Fig. S11) and the spectrum for FF-PNTs with Ag NPs but with no probe molecules (Fig. S12) show Raman spectral features assigned to vibrational modes from the FF-PNTs. Upon flexing, an increase in Raman intensity was seen in both cases (Figs. S11 and S12); however, Raman intensity was higher in the presence of Ag NPs (5-fold increase) in comparison to a 3-fold increase with FF-PNTs only. In addition to the higher Raman signal intensities, fluctuation or blinking of the Raman intensity was observed. Such blinking-based processes potentially arise from charging of the FF-PNT.[25–29] These results further support the assertion that the FF-PNTs become piezoelectrically charged during substrate bending.

The reproducibility of Raman signals from a SERS substrate is of great importance for practical use.[1–4,34] SERS spectra of 4-ABT on the template collected from randomly selected acquisition points during flexing showed ~10% changes in SERS intensity over the sample, indicating a highly uniform substrate (Fig. S13). The impact of hundreds of repeated flexing cycles (unflexed to convex flexed) on SERS signal intensities was also examined. The SERS signal stability of the FF-PNTs after different bending cycles (Figs. S13(a-d)) showed a variation of 10% (before bending) and 15%, 22%, and 25% after repeated bending of 20, 50, and 100 times or cycles, respectively, in Raman signal intensity when stress had been applied to the FF-PNTs. The overall SERS signal intensity increases with repeated flexing (Fig. S13(e)). Plotting the SERS intensity for the 1590 cm^{-1} 4-ABT band shows the signal increased during 200 flexures. The SERS spectra of 4-ABT showed an increase in Raman intensities from all bands, most notably for bands at 1420 and 1590 cm^{-1} relative to other Raman bands (Fig. S13(e-f)). Such changes in Raman band intensities are likely due to a combination of electromagnetic and chemical[30–32] enhancement mechanisms. The elevated SERS signal obtained through flexing returns to its original intensity (e.g., the intensity before the substrate was flexed) over time. The relaxation of SERS signal depends on the number of times the substrate is flexed. For instance, when flexed once, it takes around 30 minutes for the signal to retain to its original value. If the substrate is flexed 20 or 100 times, it takes 120 or 180 minutes, respectively, for the signal to revert to its original value (Fig. S13). The relaxation time appears to increase, but not scale linearly, with the number of bending cycles. Further investigation is needed to completely understand the relaxation mechanism.

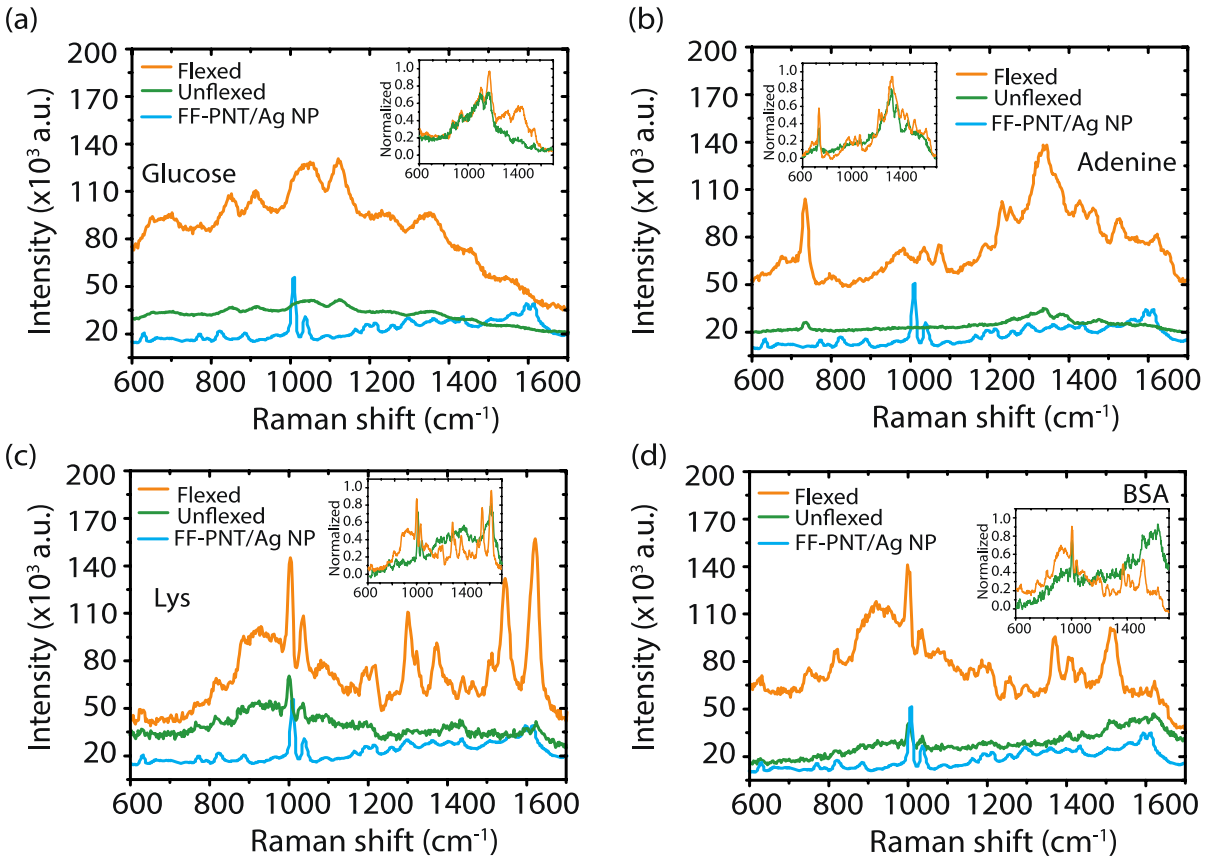

Fig. 4. SERS spectra recorded before and after convex flexing (tensile strain), with the FF-PNTs flexed to generate stress of 0.12 GPa. SERS spectra for (a) glucose (10^{-6} M), (b) adenine (10^{-6} M), (c) lysozyme (Lys) (10^{-6} M), and (d) BSA (10^{-6} M).

To demonstrate practical applications of the methodology, glucose and adenine were detected (Fig. 4(a,b)). Glucose is a simple sugar that requires monitoring in patients with diabetes. SERS detection of glucose is limited by two factors: (1) the low Raman scattering cross-section of the glucose molecule,[35,36] and (2) the poor affinity of glucose molecules to be adsorbed on metal surfaces. Fig. 4(a) shows SERS spectra of glucose on the template before and after bending. Flexing the FF-PNT/Ag NP substrate produced a significant (~10-fold) enhancement in SERS signal in comparison with an unflexed surface. The SERS spectra for glucose possess peaks located at 855 cm^{-1} (C–C stretching), 912 cm^{-1} (C–OH stretching), 1065 cm^{-1} (C–O stretching), 1126 cm^{-1} (C–O–H bending), 1365 cm^{-1} (CH_2 wagging), and 1456 cm^{-1} (CH_2 stretching), in good agreement with other reports.[35,36] It should be noted that the FF-PNT template peak located at 1603 cm^{-1} is mainly associated with aromatic vibrations, and Cα–C–N deformation.[37] The amide III FF-PNT bands are located in the range of 1220–1250 cm^{-1} and are primarily attributed to in-phase combination of N-H in-plane bending and C–N stretching vibrations. The band at 1418 cm^{-1} is assigned to the COO– symmetric stretching vibration. The intense band located at 1000 cm^{-1} corresponds to the in-plane breathing mode of the phenylalanine benzene rings. Bands at 1131 cm^{-1} are assigned to rocking vibrations of the NH_3^+ functional group.[37] Adenine also possess a low Raman cross-section making it challenging to observe directly.[38,39] Upon flexing the substrate, a clear appearance of all adenine bands (Fig. 4(b)) combined with a 7-fold increase in SERS intensity was seen (at 1350 cm^{-1}). The

Raman bands recorded in our study are in line with previous reports, showing bands located at 734, 1095, 1398, and 1641 cm^{-1}.[38,39]

Lysozyme (Lys) and bovine serum albumin (BSA) were also investigated (Fig. 4(c,d)). Lysozyme is an enzyme found in human tears. Detection of this enzyme could help protect the eye from infection. In contrast, BSA is a small, stable protein, often used in assay design (e.g., Enzyme-Linked Immunosorbent Assays) and as a protein concentration standard. In the healthy kidney, albumin's size and negative electric charge exclude it from excretion in the glomerulus.[40,41] Depending on the amount of albumin loss, a patient may have a normal renal function, microalbuminuria, or albuminuria. Therefore, the detection of albumin at low concentrations is important for accurate medical diagnosis of related diseases and their onset. For these proteins, at least a 7-fold increase in SERS intensity was seen in comparison to unflexed samples. The Raman bands recorded in our study are in line with previous reports, showing several strong peaks for Lys (Fig. 4(c)) at 938 cm^{-1} (C–C stretching), 1002 cm^{-1} (ring breathing mode due to FF-PNTs), 1240 and 1260 cm^{-1} (amide III), ~1450 cm^{-1} (C–H deformations), and 1658 cm^{-1} (amide I), and bands at 1239 and 1274 cm^{-1} (amide III), 1300 and 1450 cm^{-1} (C–H deformations), 1395 cm^{-1} (COO^- symmetric stretching), and 1650 cm^{-1} (amide I) for BSA (Fig. 4(d)). The effective detection of Lys and BSA demonstrates the applicability of the substrate to protein detection and medical assay analytics.[40,41]

Conclusions

We have successfully demonstrated for the first time a low-cost and highly sensitive and reproducible SERS substrate based on organic aligned piezoelectric diphenylalanine peptide nanotubes with silver nanoparticles on a plastic flexible substrate. Using this platform, detection of several common probe molecules and clinically-relevant proteins was demonstrated with more than an order of magnitude increase in SERS peak-to-peak ratio observed. Finite-element electromagnetics simulations revealed that the piezoelectric-based electric field induces internal fields that work cooperatively to boost the SERS signal. Thus, the signal enhancement is attributed to charge transfer between FF-PNTs and Ag NPs following the bending-induced charge generation of the piezoelectric FF-PNTs; no enhancement is observed in the absence of the FF-PNTs. Our method highlights the use of patterned self-assembling FF-PNTs in conjugate with Ag NPs for the fabrication of well-defined functional nanocomposites in the field of SERS sensing, with the potential of such materials extending to the creation of novel bio-electronic devices or microfluidic-based circuits for biomarker detection.

Experimental Details

Preparation of FF-PNT and Cyclo-dipeptide Solutions

FF-PNTs were prepared by dissolving L-diphenylalanine peptide (Bachem, Ireland) in 1,1,1,3,3,3-hexafluoro-2-propanol (Sigma-Aldrich, Ireland) at an initial concentration of 100 mg/ml and further diluting in deionized water to a final concentration of 2 mg/ml for FF-PNTs to self-assemble. Cyclo-(Phe-Phe) (Cyclo-FF, 4002860, Bachem) and Cyclo-(Trp-Trp) (Cyclo-WW, Bachem, 4011825) were dissolved in dimethyl sulfoxide (DMSO, Fischer Scientific, CAS 67-68-5) at an initial concentration of 100 mg/ml and then diluted in deionized water to concentration of 2 mg/ml. Fresh stock solutions were prepared for each experiment.

Preparation of Peptide/NP Template

FF-PNT/Ag NP and Cyclo-dipeptide/Ag NP templates were prepared using 2 mg/ml of the prepared solution heated at 100°C for 2 minutes and Ag NPs (79597, Sigma-Aldrich) with a diameter of ~40 nm at a concentration of 0.02 mg/ml in water. 20 µl of Ag NP solution was added to 60 µl of the heated solution and stirred for 3 minutes. 60 µl of the mixed solution was then deposited on the patterned flexible plastic substrate (22 x 22 mm) with thickness of 157 mm (H44690, Fisher Scientific, Ireland) to create the aligned template. The patterned regions were created by exposing the plastic flexible substrate to UV/ozone through a physical mask with an opening of 0.5 cm, following the procedure reported previously.[22,25–29] To deposit Ag NPs on a flexible substrate, 20 µl of Ag NPs (0.02 mg/ml) was diluted in 60 µl of water then 60 µl of the solution was deposited on the flexible substrate. Similarly, Au NPs (765406, Sigma-Aldrich) with a diameter of 40 nm at a concentration of 0.02 mg/ml in water were used to prepare aligned FF-PNT/Au NP templates.

Preparation of Probe Molecule Solutions

4-aminothiophenol (4-ABT) (CAS 1193-02-8, New Star Chemical) solution was prepared by dissolving 4-ABT powder in methanol to a concentration of 10^{-4} M. The solution was then further diluted with deionized water to lower concentrations**.** To prepare meso-tetra (N-methyl-4-pyridyl) porphine tetrachloride (TMPyP) (T40125, Frontier Scientific) solutions, TMPyP powder was diluted with deionized water to a final concentration of 10^{-4} M. The solution was further diluted with deionized water to a range of concentrations from 10^{-5}–10^{-11} M. Similarly, glucose (49163, Sigma-Aldrich) and adenine (A8626, Sigma-Aldrich) were prepared with deionized water (10^{-5} M or 10^{-7} M), and bovine serum albumin (A3608, Sigma-Aldrich) and human lysozyme (L1667, Sigma-Aldrich) were prepared with PBS (to an analyte concentration of 10^{-4} M) and then further diluted with deionized water to concentrations of 10^{-6} or 10^{-8} M, respectively.

UV-Vis Absorbance Spectrometer

Optical absorbance measurements of FF-PNTs with and without Ag NPs and the analyte molecule were performed on an UV-Vis absorbance spectrometer (V-650, JASCO, Inc.) under identical settings: 1 nm step size, 1 nm bandwidth, and 400 nm/minute scan speed across a 190–900 nm range. A quartz cuvette or glass cover slip was used to conduct the measurements.

Scanning Electron Microscopy (SEM)
SEM (JSM-7600F, JEOL, operated at 5 kV) was employed to characterize and observe the location of NPs decorating the surface. A thin (~ 8 nm) layer of gold was sputtered on the samples before SEM imaging (Hummer IV, Anatech USA).

Atomic Force Microscopy (AFM) and Piezoresponse Force Microscopy (PFM)
Topographic (AFM) and piezoelectric measurements of the FF-PNTs were conducted with an Asylum MFP 3D AFM. An n-type Si probe with Pt coating (HQ:CSC37/Pt) with a nominal stiffness of 0.3 N/m and nominal resonance frequency of 20 kHz was used. For PFM measurements, a 10 kHz, 30 V AC voltage, which had been amplified using a voltage amplifier (F10A, FLC Electronics AB), was applied to the AFM probe in contact with the sample. A lock-in amplifier (HF2LI, Zurich Instruments) was used to measure the in-plane piezoresponse amplitude and phase signals.

Raman Spectroscopy
SERS measurements were performed using a bespoke Raman system that consisted of an inverted optical microscope (IX71, Olympus), a monochromatic laser green laser 532 nm with beam splitter and long pass filter (RazorEdge, Semrock), a spectrograph (SP-2300i, Princeton Instruments), and a CCD camera (IXON, Andor). To focus the laser (532 nm wavelength, 5 mW incident power), a 50x objective was used. Raman spectra were collected with an exposure time of 1 s. For all Raman spectra presented, great care was taken to avoid a focusing effect by always focusing the laser on the sample surface for each measurement. 30 µl of the analyte molecule 4-ABT, TMPyP or glucose at concentration of 10^{-6} M or 10^{-11} M was deposited. Toluene was used for calibration of the Raman signal over the spectral window. SERS measurements were performed during bending the flexible substrate at a different angle. A series of SERS spectra where recorded. A series of uniformity and reproducibility tests were performed by probing different positions on the sample located between the electrodes. The peak to peak ratio was calculated through comparing the height of the Raman band of the unflexed substrate to flexed substrate. Over twenty different samples were examined and for each sample ten spectra were taken across the sample. In each case, an average of the spectra was calculated. Spectra were normalized with respect to a selected band, e.g., the spectra were normalized to the 1590 cm^{-1} band in Fig. S5.

Finite-element Electromagnetic Modelling
We used Comsol Multiphysics 5.3a to simulate a model comprising a semi-infinite FF-PNT slab interfaced to a semi-infinite air region, by solving the homogenous (source-free) Helmholtz equation. Calculations were performed both with and without an array of spherical, 40 nm Ag NPs adorning the colloid surface in a single-layer square-lattice\ configuration. The model geometry comprised a cuboid simulation cell with periodic boundary conditions applied in-plane only and comprising three layers as follows: (a) FF-PNT region volume: 40 nm x 40 nm x 200 nm; (b) air + Ag NP region volume: 40 nm x 40 nm x 41 nm; and, (c) air only volume: 40 nm x 40 nm x 100 nm. The 40 nm Ag NP is centered in the vacuum + Ag NP region, leaving a 1 nm vacuum gap between Ag and FF-PNT. For the incoming electromagnetic plane-wave, a representative incident angle with respect to normal of 36.5° was used and an incident power of 80 µW was applied.

We employed a temperature-independent complex dielectric[42] functions for the Ag NPs. For the FF-PNT substrate,[43] we used the temperature-dependent isotropic dielectric constant ε = 503 K / (435 K – T). We estimated the SERS enhancement factor G using the formula

$$G_{\mathrm{SERS}}(\lambda) = \frac{1}{A}\iint_A da \frac{|\mathbf{E}(\lambda)|^2_{\text{Ag-NP}}|\mathbf{E}(\lambda+\lambda_{\mathrm{Stokes}})|^2_{\text{Ag-NP}}}{|\mathbf{E}(\lambda)|^2_{\mathrm{bare}}|\mathbf{E}(\lambda+\lambda_{\mathrm{Stokes}})|^2_{\mathrm{bare}}},$$

where the Stokes shift was set to 40nm when applied.[44] The fourth-power law for SERS via the electromagnetic mechanism is rigorously justified in Ref. 45. We evaluated the electric field magnitude |E| on the plane positioned 0.5 nm above the colloid surface and 0.5 nm below the Ag nanoparticles, both with (Ag) and without (bare) the nanoparticle monolayer present, in separate wavelength-dependent and temperature-dependent simulations. When calculating the multiplicative SERS intensity boost due to charging, ratios of integrated enhancements G are taken. For simplicity, we focus on results for 60°C and an incident (vacuum) wavelength of 380 nm, at which we predict the SERS enhancement due to the decoration of the FF-PNTs by Ag NPs to be particularly strong for the modeled geometry. As the qualitative physics remains the same, and since we cannot expect to quantitative accuracy given the uncertainties in the FF-PNT surface coverage, we neglect the Stokes shift in the calculations shown in Fig. 3.

Acknowledgements
This research was funded by the Ministry of Higher Education of Saudi Arabia under the King Abdullah Scholarship Program (ref. no. IR10161) and Science Foundation Ireland (18/TIDA/6139, 12/IP/1556 and 07/IN1/B931). F.Z. and B.J.R acknowledge the China Scholarship Council and Science Foundation Ireland (14/US/I3113 and 17/CDA/4637). F.B. acknowledges the support of EU Horizon 2020 - Marie Skłodowska-Curie grant 713567. D.D.O'R. acknowledges Science Foundation Ireland (12/RC/2278 and 12/RC/2278 P2), and the European Regional Development Fund (ERDF). F.B. and D.D.O'R. acknowledge John F. Donegan for discussions on plasmonic materials. The authors acknowledge Ian Reid for assistance with SEM and Michael McDermott and Jim McDaid in the UCD School of Physics electronic workshop for fabricating the bending device used in the current study.

Corresponding Authors
*E-mail: james.rice@ucd.ie
*E-mail: brian.rodriguez@ucd.ie

Author Contributions
S.A., B.J.R., and J.H.R. designed the experiments and developed the experimental setup. S.A. prepared samples and performed Raman, FTIR, UV-Vis, and optical imaging. S.A. and A.F. carried out SEM measurements and created the schematics. D.A. and S.A. calculated the stress. F.Z. conducted PFM measurements. Finite-element electromagnetic modelling was performed by F.B and D.D.O'R. All authors analyzed data, discussed results, and wrote and reviewed the manuscript.

The authors declare no competing financial interest.

References

(1) Wu, W.; Liu, L.; Dai, Z.; Liu, J.; Yang, S.; Zhou, L.; Xiao, X.; Jiang, C.; Roy, V. A. L. Low-Cost, Disposable, Flexible and Highly Reproducible Screen Printed SERS Substrates for the Detection of Various Chemicals. *Sci. Rep.* **2015**, *5,* 1–10.

(2) Zuo, Z.; Zhu, K.; Gu, C.; Wen, Y.; Cui, G.; Qu, J. Transparent, Flexible Surface Enhanced Raman Scattering Substrates Based on Ag-Coated Structured PET (Polyethylene Terephthalate) for in-Situ Detection. *Appl. Surf. Sci.* **2016**, *379*, 66–72.

(3) Chen, P. X.; Shang, S. B.; Hu, L. T.; Liu, X. Y.; Qiu, H. W.; Li, C. H.; Huo, Y. Y.; Jiang, S. Z.; Yang, C. A Suitable for Large Scale Production, Flexible and Transparent Surface-Enhanced Raman Scattering Substrate for in situ Ultrasensitive Analysis of Chemistry Reagents. *Chem. Phys. Lett.* **2016**, *660*, 169–175.

(4) Zhao, X.; Yu, J.; Zhang, C.; Chen, C.; Xu, S.; Li, C.; Li, Z. Applied Surface Science Flexible and Stretchable SERS Substrate Based on a Pyramidal PMMA Structure Hybridized with Graphene Oxide Assivated AgNPs. *Appl. Surf. Sci.* **2018**, *455*, 1171–1178.

(5) Li, H.; Dai, H.; Zhang, Y.; Tong, W.; Gao, H.; An, Q. Surface-Enhanced Raman Spectra Promoted by a Finger Press in an All-Solid-State Flexible Energy Conversion and Storage Film. *Angew. Chemie - Int. Ed.* **2017**, *56*, 2649–2654.

(6) Yilmaz, M.; Babur, E.; Ozdemir, M.; Gieseking, R. L.; Dede, Y.; Tamer, U.; Schatz, G. C.; Facchetti, A.; Usta, H.; Demirel, G. Nanostructured Organic Semiconductor Films for Molecular Detection with Surface-Enhanced Raman Spectroscopy. *Nat. Mater.* **2017**, *16*, 918–924.

(7) Gao, X.; Matsui, H. Peptide-Based Nanotubes and Their Applications in Bionanotechnology. *Adv. Mater.* **2005**, *17* (17), 2037–2050. https://doi.org/10.1002/adma.200401849.

(8) Yemini, M.; Reches, M.; Rishpon, J.; Gazit, E. Novel Electrochemical Biosensing Platform Using Self-Assembled Peptide Nanotubes. *Nano Lett.* **2005**, *5*, 183–186.

(9) Kol, N.; Adler-abramovich, L.; Barlam, D.; Shneck, R. Z. Self-Assembled Peptide Nanotubes Are Uniquely Rigid Bioinspired Supramolecular Structures. **2005**, *Nano Lett*, 2005, 5, 1343–1346.

(10) Azuri, I.; Adler-abramovich, L.; Gazit, E.; Hod, O.; Kronik, L. Why Are Diphenylalanine-Based Peptide Nanostructures so Rigid ? Insights from First Principles Calculations. *J. Am. Chem. Soc.* **2014**, *136*, 963–969.

(11) Almohammed, S.; Alruwaili, M.; Reynaud, E. G.; Redmond, G.; Rice, J. H.; Rodriguez, B. J. 3D-Printed Peptide-Hydrogel Nanoparticle Composites for Surface-Enhanced Raman Spectroscopy Sensing. *ACS Appl. Nano Mater.* **2019**, 2, 5029–5034.

(12) Adler- Abramovich, L.; Reches, M.; Sedman, V. L.; Allen, S.; Tendler, S. J. B.; Gazit, E. Thermal and Chemical Stability of Diphenylalanine Peptide Nanotubes:Implications for Nanotechnological Applications. *Langmuir* **2006**, *22*, 1313–1320.

(13) Esin, A.; Baturin, I.; Nikitin, T.; Vasilev, S.; Salehli, F.; Shur, V. Y.; Kholkin, A. L. Pyroelectric Effect and Polarization Instability in Self-Assembled Diphenylalanine Microtubes. *Appl. Phys. Lett.* **2016**, *109*, 1–5.

(14) Zhang, Y.; Xie, M.; Roscow, J.; Bao, Y.; Zhou, K.; Zhang, D.; Bowen, C. R.

Enhanced Pyroelectric and Piezoelectric Properties of PZT with Aligned Porosity for Energy Harvesting Applications. *J. Mater. Chem. A* **2017**, *5*, 6569–6580.
(15) Kholkin, A.; Amdursky, N.; Bdikin, I.; Gazit, E.; Rosenman, G. Strong Piezoelectricity in Bioinspired Peptide Nanotubes. *ACS Nano* **2010**, *4*, 610–614.
(16) Adler-abramovich, L.; Gazit, E. The Physical Properties of Supramolecular Peptide Assemblies: From Building Block Association to Technological Applications. *Chem. Soc. Rev.* **2014**, *43*, 6881–6893.
(17) Damm, S.; Carville, N. C.; Rodriguez, B. J.; Manzo, M.; Gallo, K.; Rice, J. H. Plasmon Enhanced Raman from Ag Nanopatterns Made Using Periodically Poled Lithium Niobate and Periodically Proton Exchanged Template Methods. *J. Phys. Chem. C* **2012**, *116*, 26543–26550.
(18) Chang, J.; Dommer, M.; Chang, C.; Lin, L. Piezoelectric Nanofibers for Energy Scavenging Applications. *Nano Energy* **2012**, *1*, 356–371.
(19) Lee, J.H.; Heo, K.; Schulz-Schönhagen, K.; Lee, J. H.; Desai, M. S.; Jin, H.-E.; Lee, S.W. Diphenylalanine Peptide Nanotube Energy Harvesters. *ACS Nano* **2018**, *8*, 8138–8144.
(20) Jenkins, K.; Kelly, S.; Nguyen, V.; Wu, Y.; Yang, R. Piezoelectric Diphenylalanine Peptide for Greatly Improved Flexible Nanogenerators. *Nano Energy* **2018**, *51*, 317–323.
(21) Nguyen, V.; Zhu, R.; Jenkins, K.; Yang, R. Self-Assembly of Diphenylalanine Peptide with Controlled Polarization for Power Generation. *Nat. Commun.* **2016**, *7*, 13566.
(22) Almohammed, S.; Oladapo, S. O.; Ryan, K.; Kholkin, A. L.; Rice, J. H.; Rodriguez, B. J. Wettability Gradient-Induced Alignment of Peptide Nanotubes as Templates for Biosensing Applications. *RSC Adv.* **2016**, *6*, 41809–41815.
(23) Lin, T. Y.; Pfeiffer, T. T.; Lillehoj, P. B. Stability of UV/Ozone-Treated Thermoplastics under Different Storage Conditions for Microfluidic Analytical Devices. *RSC Adv.* **2017**, *7*, 37374–37379.
(24) Luo, S.; Wong, C. P. Effect of UV Ozone Treatment on Surface Tension. IEEE Transactions on components and packaging Technologies,**2001**, *24* (1), 43–49.
(25) Almohammed, S.; Fedele, S.; Rodriguez, B. J.; Rice, J. H. Aligned Diphenylalanine Nanotube – Silver Nanoparticle Templates for High - Sensitivity Surface - Enhanced Raman Scattering. *J. Raman Spectrosc*. 2017, 48, 1799–1807.
(26) Almohammed, S.; Zhang, F.; Rodriguez, B. J.; Rice, J. H. Photo-Induced Surface-Enhanced Raman Spectroscopy from a Diphenylalanine Peptide Nanotube-Metal Nanoparticle Template. *Sci. Rep.* **2018**, *8*, 3880.
(27) Almohammed, S.; Tade Barwich, S.; Mitchell, A. K.; Rodriguez, B. J.; Rice, J. H. Enhanced Photocatalysis and Biomolecular Sensing with Field-Activated Nanotube-Nanoparticle Templates. *Nat. Commun.* **2019**, *10*, 2496.
(28) Almohammed, S.; Zhang, F.; Rodriguez, B. J.; Rice, J. H. Electric Field-Induced Chemical SERS Enhancement from Aligned Peptide Nanotube–Graphene Oxide Templates for Universal Trace Detection of Biomolecules. *J. Phys. Chem. Lett.* **2019**, 10, 1878-1887.
(29) Almohammed, S.; Rodriguez, B. J.; Rice, J. H. Nucleobase Sensing Using Highly-Sensitive Surface-Enhanced Raman Spectroscopy Templates Comprising Organic Semiconductor Peptide Nanotubes and Metal

Nanoparticles. *Sens. Bio-Sensing Res.* **2019**, *24*, 100287.
(30) De Barros Santos, E.; Sigoli, F. A.; Mazali, I. O. Intercalated 4-Aminobenzenethiol between Au and Ag Nanoparticles: Effects of Concentration and Nanoparticles Neighborhood on Its SERS Response. *J. Braz. Chem. Soc.* **2015**, *26*, 970–977.
(31) Santos, E. D. B.; Sigoli, F. A.; Mazali, I. O. Surface-Enhanced Raman Scattering of 4-Aminobenzenethiol on Silver Nanoparticles Substrate. *Vib. Spectrosc.* **2013**, *68*, 246–250.
(32) Osawa, M.; Matsuda, N.; Yoshii, K.; Uchida, I. Charge Transfer Resonance Raman Process in Surface-Enhanced Raman Scattering from p-Aminothiophenol Adsorbed on Silver: Herzberg-Teller Contribution. *J. Phys. Chem.* **1994**, *98*, 12702–12707.
(33) Šmejkal, P.; Vlčková, B.; Procházka, M.; Mojzeš, P.; Pfleger, J. Testing Anionic Spacers by SERRS (Surface-Enhanced Resonance Raman Scattering) of a Cationic Free-Base Porphyrin in Systems with Laser-Ablated Ag Colloids. *Vib. Spectrosc.* **1999**, *19*, 243–247.
(34) Zhang, C.; Yi, P.; Peng, L.; Lai, X.; Chen, J.; Huang, M.; Ni, J. Continuous Fabrication of Nanostructure Arrays for Flexible Surface Enhanced Raman Scattering Substrate. *Sci. Rep.* **2017**, *7*, 1–9.
(35) Sooraj, K. P.; Ranjan, M.; Rao, R.; Mukherjee, S. Applied Surface Science SERS Based Detection of Glucose with Lower Concentration than Blood Glucose Level Using Plasmonic Nanoparticle Arrays. *Appl. Surf. Sci.* **2018**, *447*, 576–581.
(36) Ju, J.; Liu, W.; Perlaki, C. M.; Chen, K.; Feng, C.; Liu, Q. Sustained and Cost Effective Silver Substrate for Surface Enhanced Raman Spectroscopy Based Biosensing. *Sci. Rep.* **2017**, *7*, 1–11.
(37) Sereda, V.; Ralbovsky, N. M.; Vasudev, M. C.; Naik, R. R.; Lednev, I. K. Polarized Raman Spectroscopy for Determining the Orientation of Di-d-Phenylalanine Molecules in a Nanotube. *J. Raman Spectrosc.* **2016**, *47*, 1056–1062.
(38) Ten, G. N.; Burova, T. G.; Baranov, V. I. Calculation and Analysis of Vibrational Spectra of Adenine – Thymine , Guanine – Cytosine , and Adenine – Uracil Complementary Pairs in the Condensed State. **2009**, *76* (1), 84–92.
(39) Madzharova, F.; Heiner, Z.; Guhlke, M.; Kneipp, J. Surface-Enhanced Hyper-Raman Spectra of Adenine, Guanine, Cytosine, Thymine, and Uracil. *J. Phys. Chem. C* **2016**, *120* (28), 15415–15423.
(40) Fazio, B.; Andrea, C. D.; Foti, A.; Messina, E.; Irrera, A.; Donato, M. G.; Villari, V.; Micali, N.; Maragò, O. M.; Gucciardi, P. G. SERS Detection of Biomolecules at Physiological PH via Aggregation of Gold Nanorods Mediated by Optical Forces and Plasmonic Heating. *Nat. Publ. Gr.* **2016**, *6*,1–13.
(41) Xiaodan, W.; Dawei, Z.; Ping, Z.; Taifeng, L.; Huiqin, W.; Yongwei, Z. Surface-Enhanced Raman Scattering Investigation of Bovine Serum Albumin by Au Nanoparticles with Different Sizes. *J. Appl. Biomater. Funct. Mater.* **2018**, *16*, 157–162.
(42) Rakić, A. D.; Djurišic, A. B.; Elazar, J. M.; Majewski, M. L. Optical properties of metallic films for vertical-cavity optoelectronic devices. Applied Optics **1998**, *37*, 5271–5283.
(43) Bdikin, I.; Bystrov, V.; Kopyl, S.; Lopes, R. P. G.; Delgadillo, I.; Gracio, J.; Mishina, E.; Sigov, A.; Kholkin, A. L. Evidence of Ferroelectricity and Phase Transition in Pressed Diphenylalanine Peptide Nanotubes. *Appl. Phys. Lett.*

2012, *100*, 043702.
(44) Knorr, I.; Christou, K.; Meinertz, J. Prediction and Optimization of Surface-Enhanced Raman Scattering Geometries Using COMSOL Multiphysics. *Procedings COMSOL Conf.* **2008**, 1–7.
(45) Le Ru, E. C.; Etchegoin, P. G. Rigorous justification of the |E|^4 enhancement factor in Surface Enhanced Raman Spectroscopy. *Chem. Phys. Lett.* **2006** 423, 63–66.

Supporting Information

Flexing piezoelectric diphenylalanine–plasmonic metal nanocomposites to increase SERS signal strength

Sawsan Almohammed [a, b], Agata Fularz [a], Fengyuan Zhang [a, b], Diana Alvarez-Ruiz [a], Frank Bello [c], David D. O'Regan [c], Brian J. Rodriguez * [a, b], and James H. Rice * [a]

[a]*School of Physics, University College Dublin, Belfield, Dublin 4, Ireland*
[b]*Conway Institute of Biomolecular and Biomedical Research, University College Dublin, Belfield, Dublin 4, Ireland*
[c]*School of Physics, AMBER and CRANN Institute, Trinity College Dublin, The University of Dublin, Dublin 2, Ireland*

Corresponding Authors
*E-mail: james.rice@ucd.ie.
*E-mail: brian.rodriguez@ucd.ie.

Substrate characterization

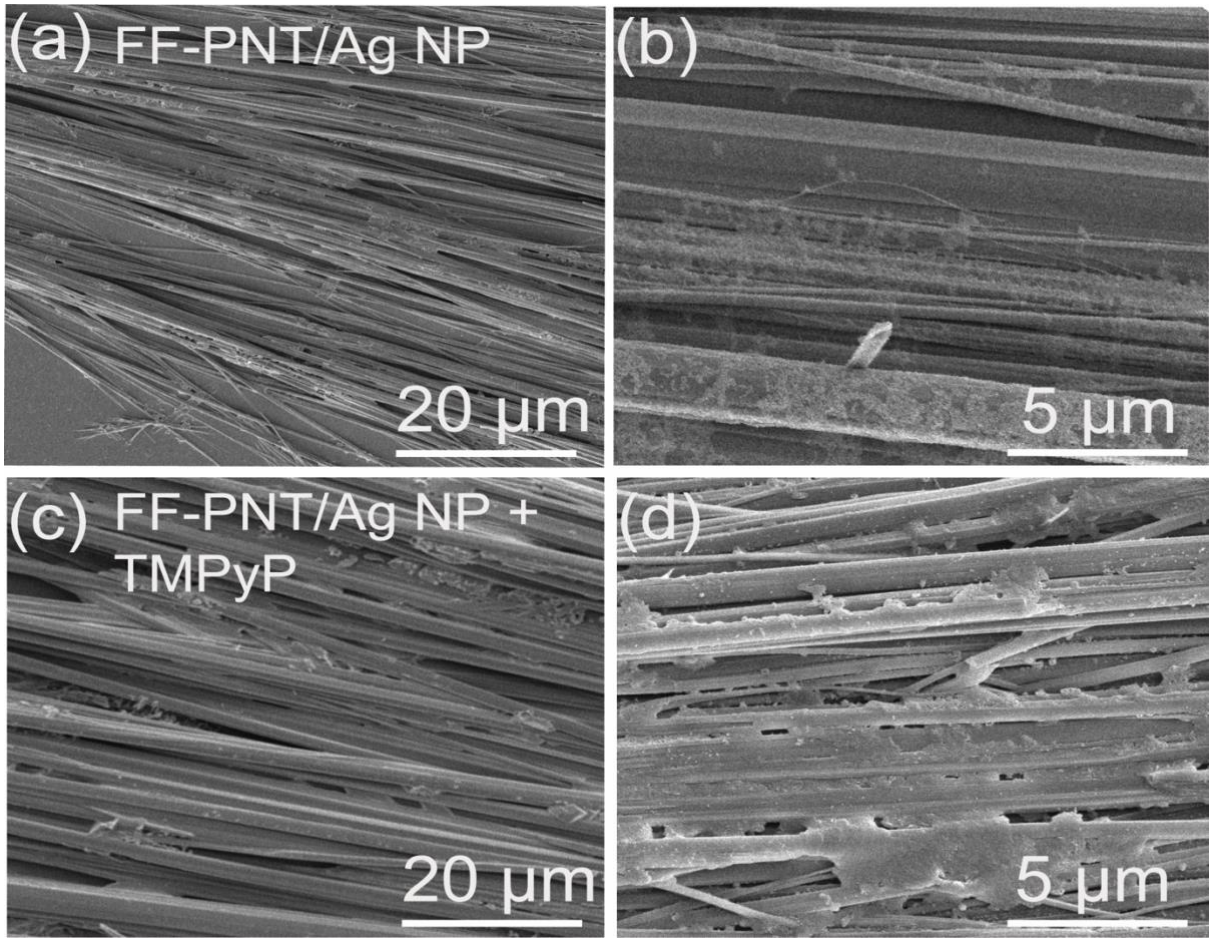

Figure S1. (a, b) SEM images of aligned FF-PNT/Ag NP substrates. (c, d) SEM images of aligned FF-PNT/Ag NP substrates after the addition of TMPyP.

A Scanning electron microscope (SEM; TM4000Plus Tabletop Microscope, Hitachi, operated at 15 kV) equipped with energy-dispersive X-ray spectroscopy (EDX; Oxford Instruments) was employed to characterize the samples. A thin (~10 nm) layer of gold was sputtered (EMITECH K575X sputter coater) on the samples before SEM imaging. SEM images of the FF-PNT/Ag NP substrates before and after the addition of probe molecule TMPyP are shown in Fig. S1. The same sample was imaged by EDX before and after flexing for comparison (Fig. S2).

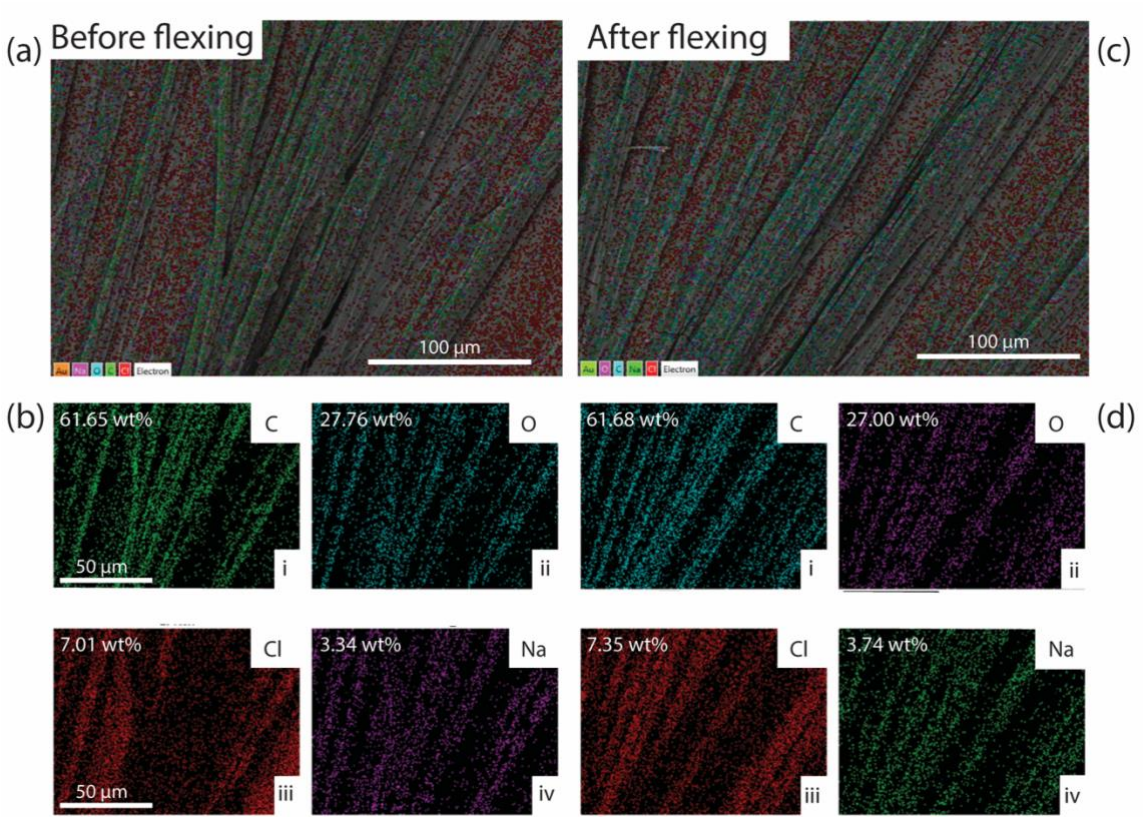

Figure S2. EDX mapping of the template (a, b) before and (c, d) after bending 100 convex bending cycles (0.12 GPa), showing that the FF-PNTs remain chemically similar. Note that labels in the bottom left corners of (a, c) are different.

Compressive and tensile stress calculations

Bending the nanocomposites generates both compressive and tensile strains, $\varepsilon_x = \pm Y/\rho$, of equal magnitude on the top and bottom surfaces of the sample, respectively,[1] where Y is the distance from the neutral axis to the surface of the sample and ρ is the radius of curvature after bending. Assuming a uniaxial compression/tension, the bending stress can be calculated from $\sigma_x = E\varepsilon_x$, where E is the (estimated) Young's modulus of the composite. Table S1 shows the calculated bending stress for six different radii of curvature.

Table S1. Calculation of the stress during flexing.

Radius of curvature (mm)	Stress (GPa)
0	0
41.7	0.03772
20.5	0.07681
13.6	0.11547
10.4	0.15038
8.9	0.17561
8.6	0.18186
8.3	0.19785

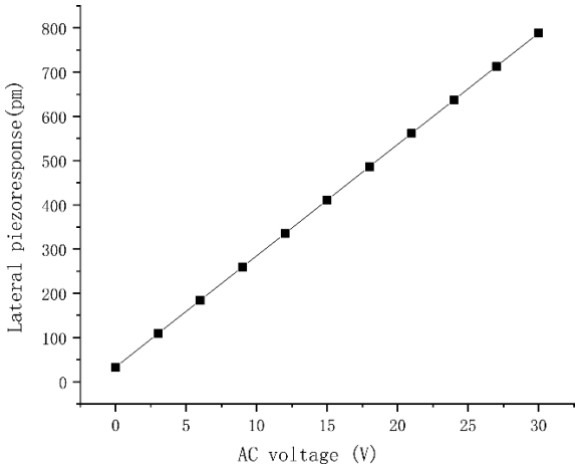

Figure S3. A plot of the dependence of lateral PFM amplitude on the applied voltage. The slope of the linear fit provides the effective d_{15} piezoelectric coefficient. The average d_{15} for FF-PNTs was determined to be 27.5 ± 0.4 pm/V (n = 5 locations), which is comparable to values reported elsewhere.[2]

UV-Vis absorption

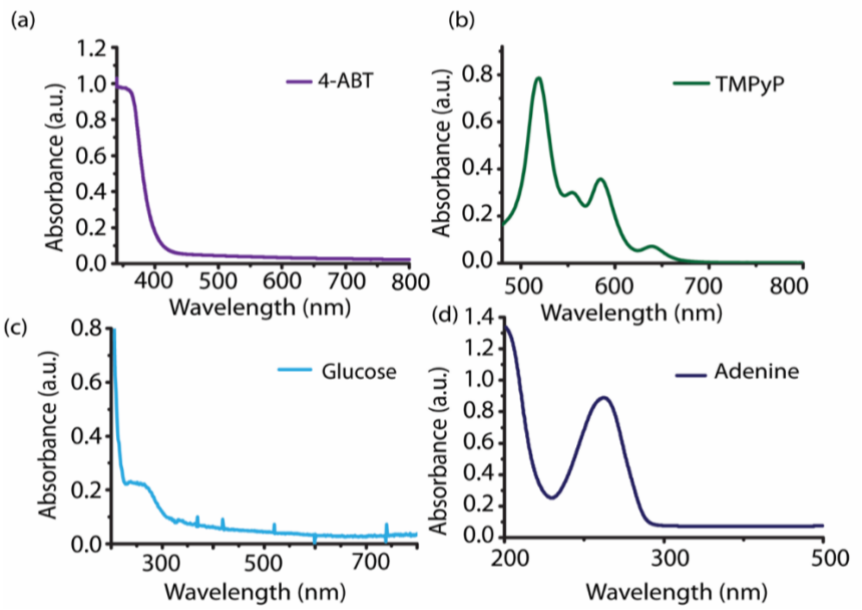

Figure S4. UV-Vis absorption spectra of the probe molecules studied. (a) Absorption spectra of 4-ABT (10^{-4} M). (b) Absorption spectra of TMPyP (10^{-4} M). (c) Absorption spectra of glucose (10^{-4} M). (d) Absorption spectra of adenine (10^{-4} M).

SERS spectra

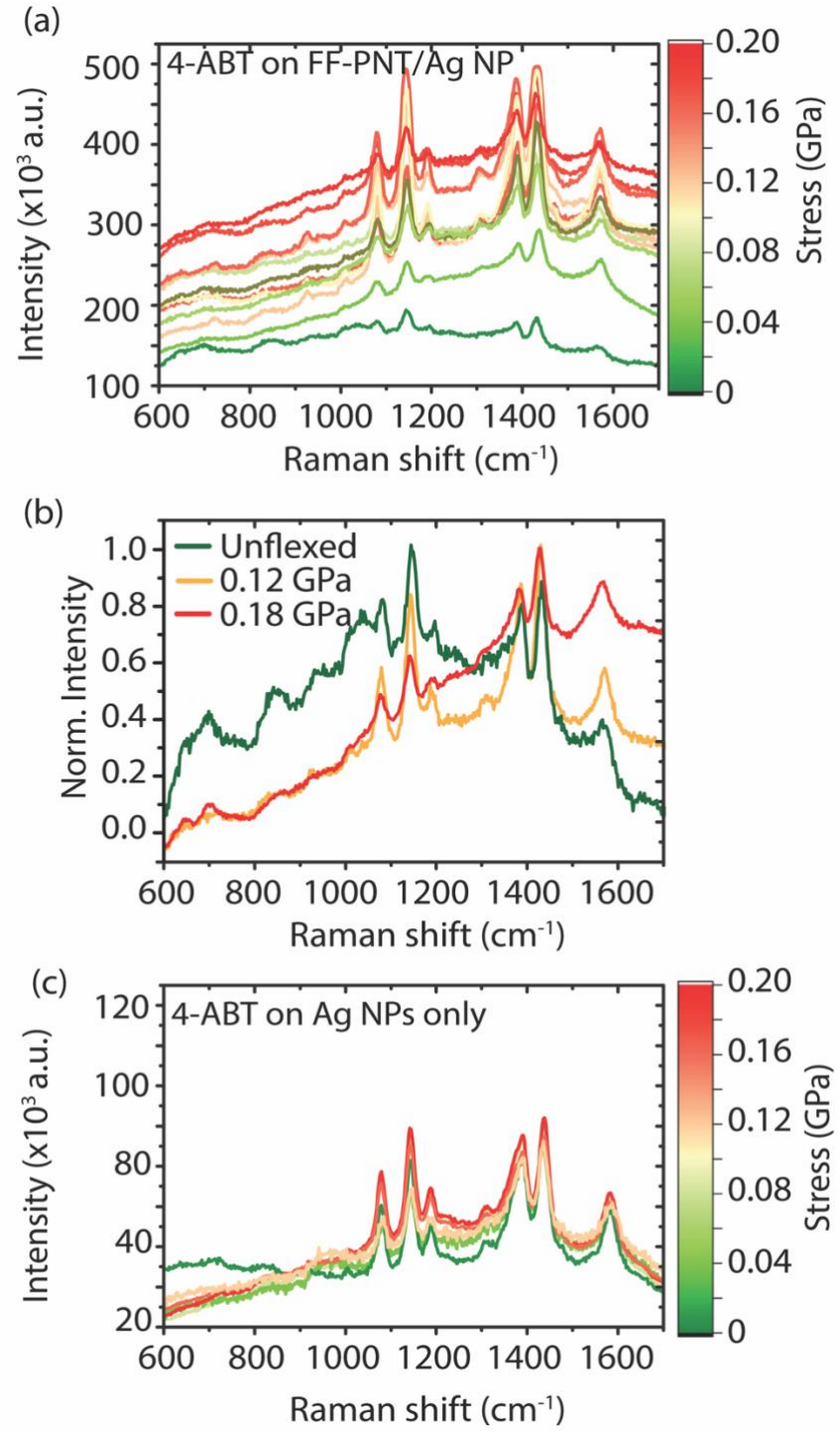

Figure S5. (a) SERS measurements of 10^{-6} M 4-ABT on an aligned FF-PNT/Ag NP flexible substrate recorded as a function of stress. Bending the substrate in an upward direction as shown in Fig. 2(d), main paper. (b) Normalized spectra (from (a)) of 4-ABT on the flexible template with and without bending. (c) SERS spectra of 10^{-6} M 4-ABT on Ag NPs on a flexible substrate in the absence of FF-PNTs.

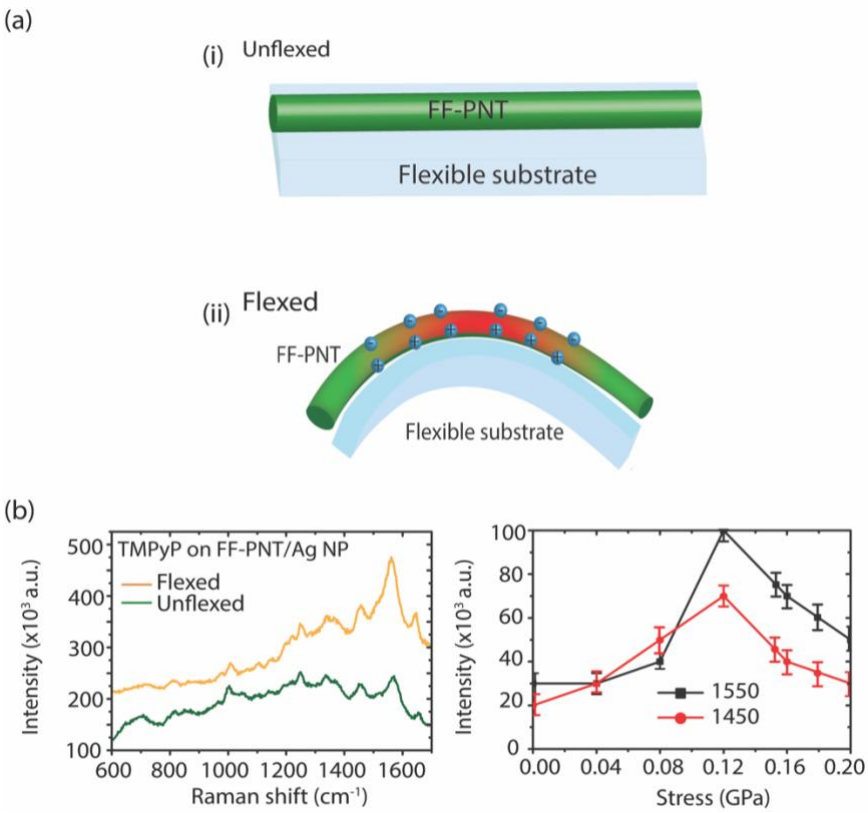

Figure S6. SERS measurements of the probe molecule TMPyP on an aligned FF-PNT/Ag NP flexible substrate recorded as a function of stress. (a) Schematic drawings of the (i) unflexed and (ii) flexed substrate. Shown in red (in ii) is the area where the generated stress is maximized. (b) SERS spectra recorded before and after flexing, with the FF-PNTs flexed to generate a stress of 0.12 GPa (left). Plot of SERS signal intensity versus generated stress for two peaks (right).

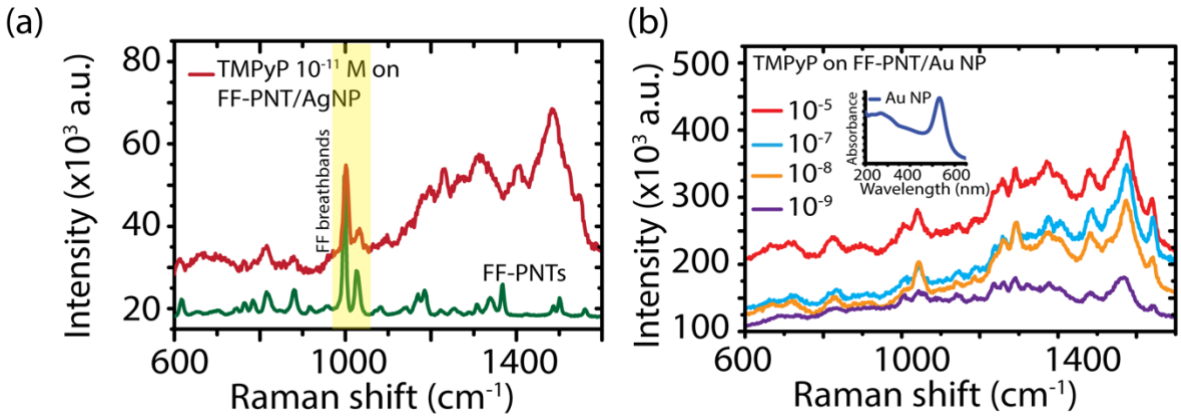

Figure S7. (a) SERS measurements of TMPyP at 10^{-11} M concentration on aligned FF-PNT flexible templates with Ag NPs flexed to generate a stress of 0.12 GPa. (b) SERS measurements of TMPyP at 10^{-5} M to 10^{-9} M concentrations on aligned FF-PNT flexible templates with Au NPs flexed to generate a stress of 0.12 GPa. The inset in (b) is the absorption spectra of Au NPs showing an SPR at ~580 nm.

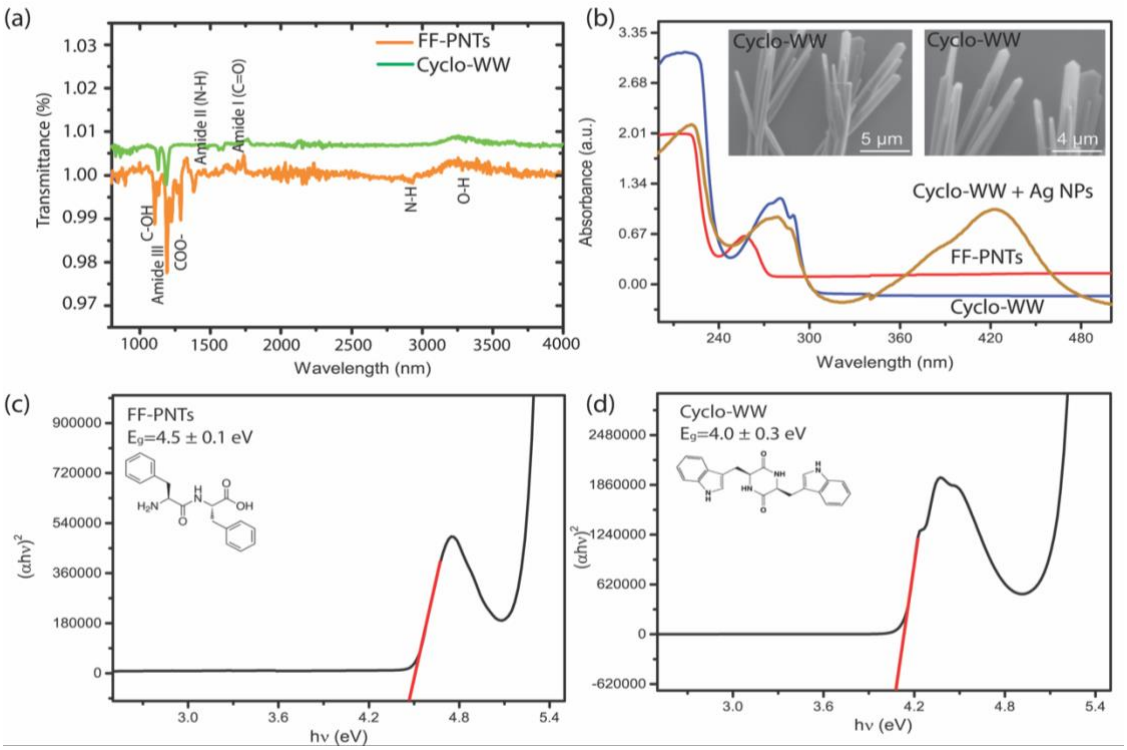

Figure S8. (a) FTIR measurements of FF-PNTs and Cyclo-WW. (b) UV-Vis of FF-PNTs and Cyclo-WW; SEM images of the Cyclo-WW structures in inset. (c-d) Band gap calculation from UV-Vis data in (b) showing that FF-PNTs have a band gap of around 4.5 eV, in comparison to 4.0 eV for Cyclo-WW.

Studies have shown that the properties of non-centrosymmetric FF-PNTs differ from orthorhombic Cyclo-FF structures.[3–6] We have characterized both Cyclo-WW and Cyclo-FF using FTIR, SEM, and UV-Vis, as shown in Figs. S8 and S9. FTIR modes at 1730 nm and 3400 nm and modes from 1380–1460 nm are attributed to the stretching of C=O bonds, O–H bonds, and the stretching modes of the C–OH bonds of carbonyl and carboxylic acid, respectively. The Amide I band at 1654 and the Amide II bands at 1530 and 1547 nm indicate an alpha helix structure. The Amide III band at 1308 nm and the N-H stretching at 3319 nm and 3266 nm correspond to hydrogen bonding, in agreement with literature reports.[3–6]

Cyclo-WW formed needle-like structures with a diameter of 2.5 ± 1.3 µm (n = 30), as shown in the inset of Fig. S8(b). FF-PNTs have an absorption band located at 220 nm, indicative of a π–π* electronic transition of the phenylalanine ring with subpeaks at 265 nm (4.68 eV) and 253 nm (4.90 eV) arising from the aromatic residues (Fig. S8(b)).[7] The band at 253 nm slightly red-shifted, as expected for Cyclo-WW.[7] Once incorporated with Ag NPs, bands located at ~420 nm can be seen for Cyclo-WW, which are attributed to surface plasmon resonance of the Ag NPs. The lower bandgap of Cyclo-WW in comparison to FF-PNTs could be due to the increased hydrogen bonding and aromatic interactions, as shown in Fig. S8(c, d).

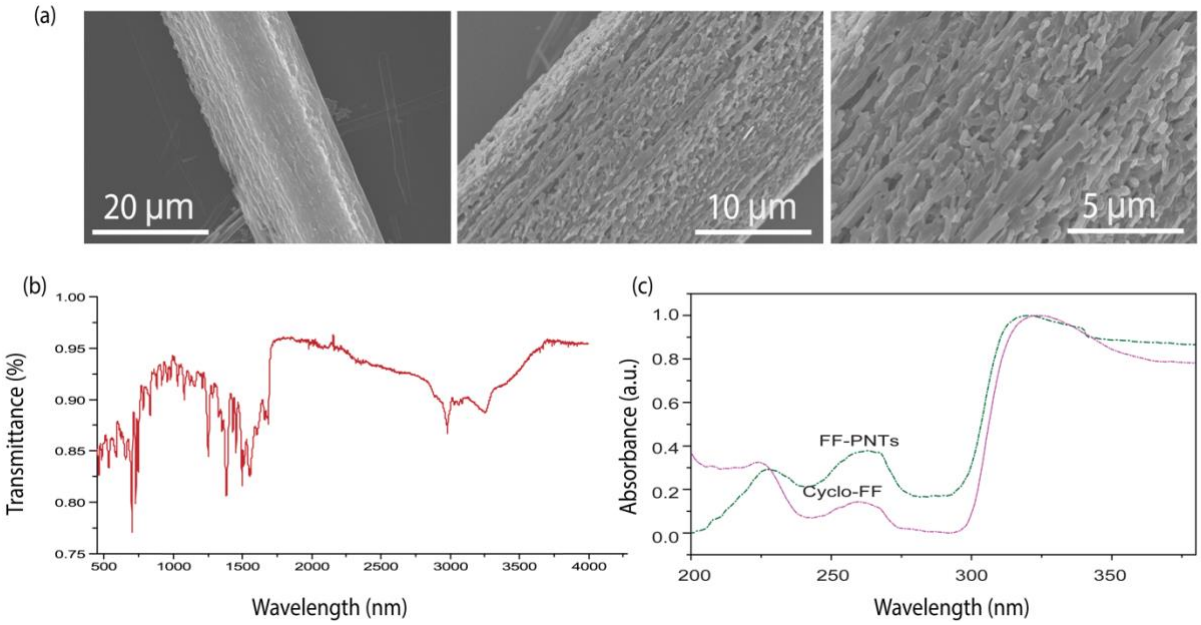

Figure S9. (a) SEM images and (b) FTIR spectra of orthorhombic Cyclo-FF. (c) UV-Vis absorbance of Cyclo-FF and FF-PNTs.

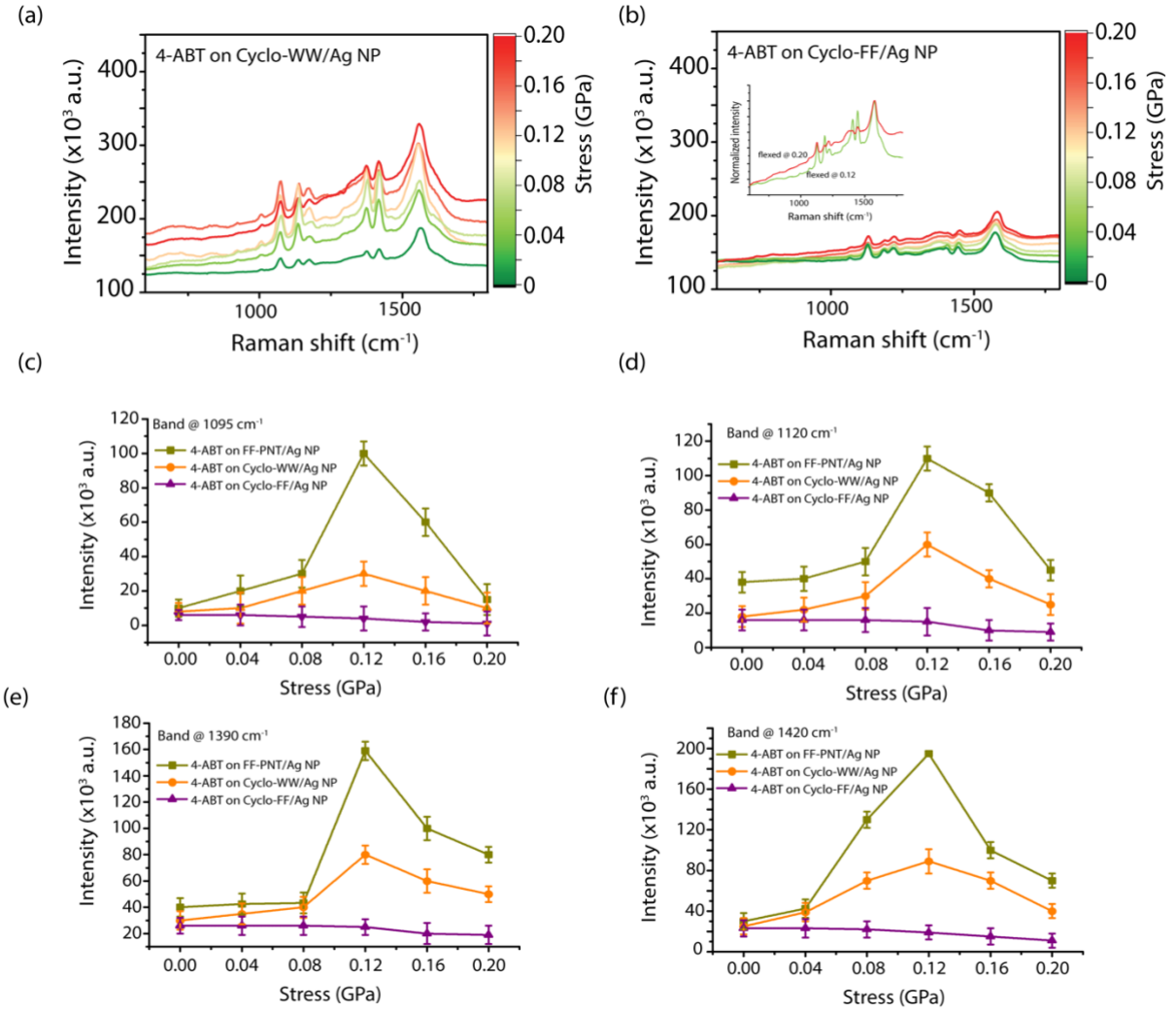

Figure S10. Studies comparing piezoelectric FF-PNTs, low-piezoelectric Cyclo-WW, and non-piezoelectric Cyclo-FF. SERS measurements of the probe molecule 4-ABT (10^{-6} M) using (a) the Cyclo-WW/Ag NP flexible substrate and (b) the Cyclo-FF/Ag NP flexible substrate. The inset in (b) shows normalized SERS spectra of 4-ABT on the Cyclo-FF-Ag NPs template at low and high stress, showing significant reduction of 4-ABT bands, especially at 1390 cm^{-1} and 1420 cm^{-1}. (c-f) Plots of SERS signal intensity versus the degree of strain when using FF-PNTs vs Cyclo-WW or Cyclo-FF with 4-ABT.

These data (Figs. S8–S10) show that the low or non-piezoelectric peptide nanotubes do not enhance the SERS signal to the same extent as when the piezoelectric peptides are applied. The lowest enhancement was recorded with flexing when using Cyclo-FF (orthorhombic non-piezoelectric materials), by which no significant changes in peak-to-peak ratio was observed (only a slight change in the background). However, the slight increase or enhancement in SERS intensity with Cyclo-WW could be due to the fact that it has smaller band gap than FF-PNTs, as shown Fig. S6, features that can be explored in future work as having a smaller band gap makes them more easily excited.

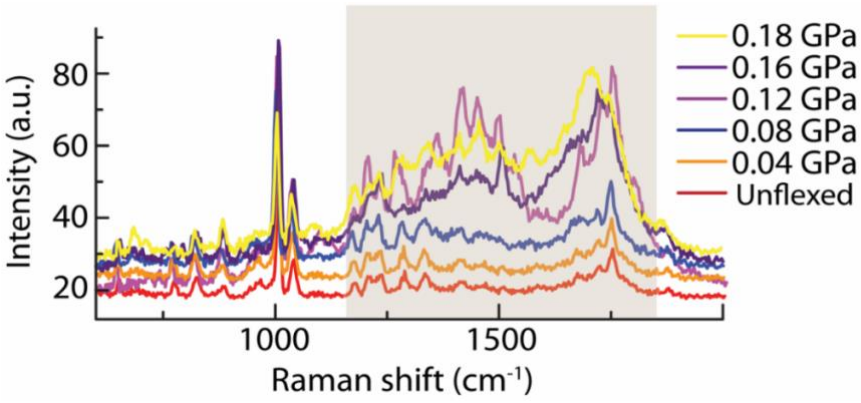

Figure S11. SERS spectra taken from aligned FF-PNT flexible substrate with no probe molecule and no Ag NPs present. SERS recorded as a function of stress.

The shading (Fig. S11) shows a region where the FF-PNT bands change, which could be due to rotation of FF molecules within FF-PNTs with respect to the incident laser when the FF-PNTs are bending.[9,10]

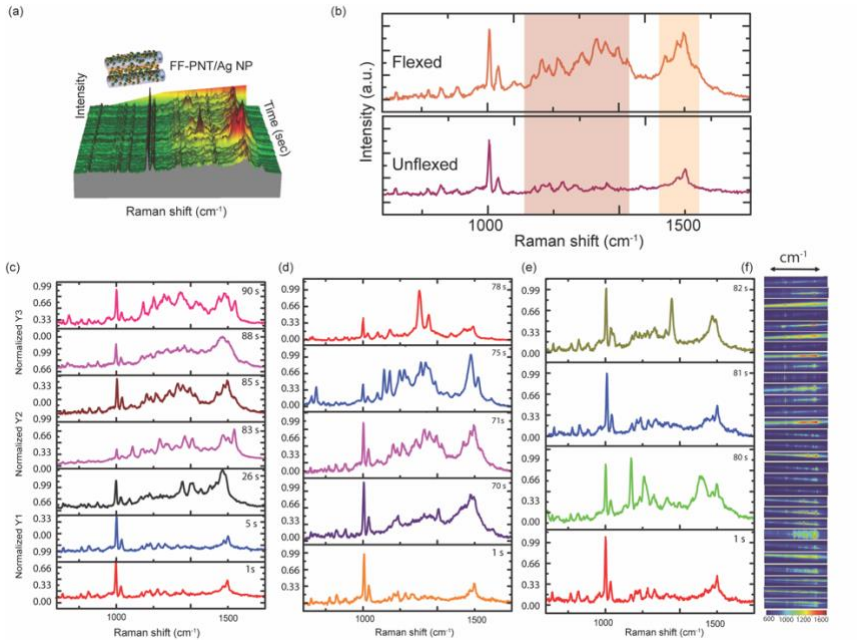

Figure S12. SERS measurements taken from an aligned FF-PNT/Ag NP flexible substrate with no probe molecules present. (a) A 3D plot of SERS spectra after 50 bending cycles (unflexed to convex flexed) with the FF-PNTs flexed to generate stress of 0.12 GPa. (b) SERS measurements during and after bending (cycle 1). (c-f) Separate recorded series of SERS spectra showing SERS blinking after 50 bending cycles with the FF-PNTs flexed to generate stress of 0.12 GPa.

Nearly all FF-PNT bands were detectable on the flexible substrate with and without bending such as the aromatic ring breathing mode at 1002 cm^{-1} and a phenyl vibrational band at 1603 cm^{-1}. Modes at 1249 cm^{-1} corresponding to amide III

vibrations are seen, which indicate strong coupling between C_α–H and N−H bending vibrations, in agreement with density functional theory calculations used to assign FF-PNT Raman modes.[9–12] The intensity of the amide I mode (1670 cm^{-1}) can be used to determine the orientation of the carbonyl groups in FF-PNTs with respect to the nanotube axis. The amide I Raman band is mainly attributed to a C=O stretching vibrational mode along with C–N stretching and C_α–C–N deformation. The amide I frequency (1670 cm^{-1}) indicates that only N−H is involved in hydrogen bonding. The Raman band at 1418 cm^{-1} (assigned to the symmetric stretching vibration) also showed a strong polarization effect.[9–12] The intense band located at 1002 cm^{-1} corresponding to the in-plane breathing mode of the phenylalanine benzene rings increased linearly with bending.

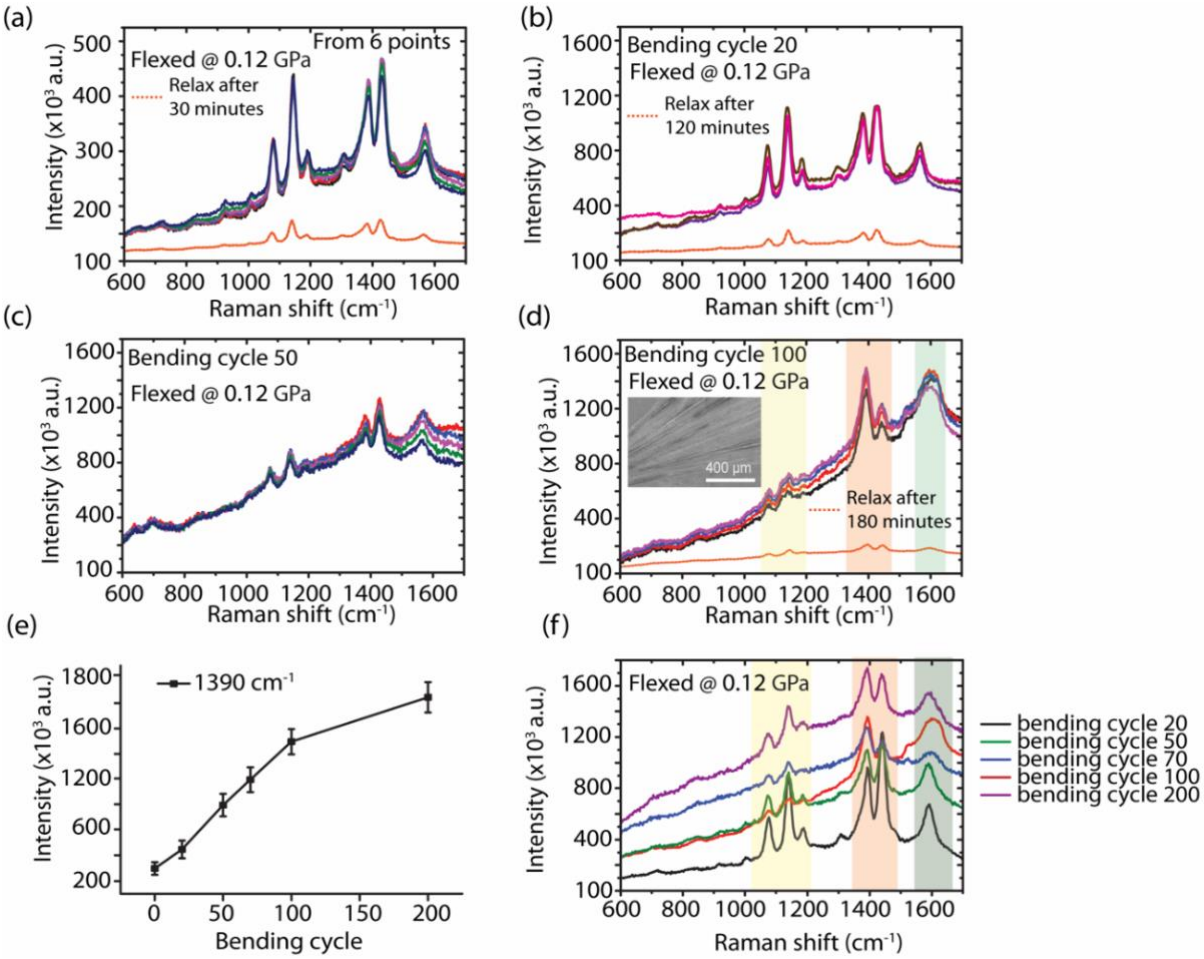

Figure S13. SERS measurements taken from 10^{-6} M 4-ABT on an aligned FF-PNT/Ag NP flexible substrate. (a) Uniformity test at 6 different points on the flexible template with the FF-PNTs flexed to generate stress of 0.12 GPa. Spectra after bending (b) 30 times; (c) and (d) after 50 and 100 cycles, respectively. (e) A plot of 4-ABT SERS intensity versus the bending cycle. The orange spectra in (a), (b), and (d) show relaxation of the signal over time (Relax). (f) SERS spectra for 10^{-6} M 4-ABT on an aligned FF-PNT/Ag NP flexible substrate for different bending cycles.

References

(1) Kim, S.; Choi, S. J.; Zhao, K.; Yang, H.; Gobbi, G.; Zhang, S.; Li, J. Electrochemically Driven Mechanical Energy Harvesting. *Nat. Commun.* **2016**, *7*, 10146.

(2) Lee, J.H.; Heo, K.; Schulz-Schönhagen, K.; Lee, J. H.; Desai, M. S.; Jin, H.-E.; Lee, S.-W. Diphenylalanine Peptide Nanotube Energy Harvesters. *ACS Nano* **2018**, *8*, 8138–8144.

(3) Tao, K.; Fan, Z.; Sun, L.; Makam, P.; Tian, Z.; Ruegsegger, M.; Shaham-Niv, S.; Hansford, D.; Aizen, R.; Pan, Z.; et al. Quantum Confined Peptide Assemblies with Tunable Visible to Near-Infrared Spectral Range. *Nat. Commun.* **2018**, *9* (1), 1–11.

(4) Akdim, B.; Pachter, R.; Naik, R. R. Self-Assembled Peptide Nanotubes as Electronic Materials: An Evaluation from First-Principles Calculations. *Appl. Phys. Lett.* **2015**, *106* (18), 183707.

(5) Handelman, A.; Natan, A.; Rosenman, G. Structural and Optical Properties of Short Peptides: Nanotubes-to-Nanofibers Phase Transformation. *J. Pept. Sci.* **2014**, *20* (7), 487–493.

(6) Amdursky, N.; Handelman, A.; Rosenman, G. Optical Transition Induced by Molecular Transformation in Peptide Nanostructures. *Appl. Phys. Lett.* **2012**, *100* (10), 103701.

(7) Kogikoski, S.; Khanra, S.; Alves, W. A.; Guha, S. SERS Active Self-Assembled Diphenylalanine Micro/Nanostructures: A Combined Experimental and Theoretical Investigation. *J. Chem. Phys.* **2017**, *147* (8), 084703.

(8) Tao, K.; Xue, B.; Li, Q.; Hu, W.; Shimon, L. J. W.; Makam, P.; Si, M.; Yan, X.; Zhang, M.; Cao, Y.; et al. Stable and Optoelectronic Dipeptide Assemblies for Power Harvesting. *Mater. Today* **2019**, *30*, 10–16.

(9) Sereda, V.; Ralbovsky, N. M.; Vasudev, M. C.; Naik, R. R.; Lednev, I. K. Polarized Raman Spectroscopy for Determining the Orientation of di-D-Phenylalanine Molecules in a Nanotube. *J. Raman Spectrosc.* **2016**, *47* (9), 1056–1062.

(10) Almohammed, S.; Fedele, S.; Rodriguez, B. J.; Rice, J. H. Aligned Diphenylalanine Nanotube – Silver Nanoparticle Templates for High - Sensitivity Surface - Enhanced Raman Scattering. **2017**, 28 (12), 1799–1807.

(11) Almohammed, S.; Zhang, F.; Rodriguez, B. J.; Rice, J. H. Photo-Induced Surface-Enhanced Raman Spectroscopy from a Diphenylalanine Peptide Nanotube-Metal Nanoparticle Template. *Sci. Rep.* **2018**, *8* (1), 3880.

(12) Almohammed, S.; Oladapo, S. O.; Ryan, K.; Kholkin, A. L.; Rice, J. H.; Rodriguez, B. J. Wettability Gradient-Induced Alignment of Peptide Nanotubes as Templates for Biosensing Applications. *RSC Adv.* **2016**, *6* (48), 41809–41815.